AN ABSTRACT OF THE THESIS OF

Clare E. Reimers for the degree of Master of Science

in Oceanography presented on July 10, 1978

Title: THE FLOW MECHANICS AND RESULTING EROSIONAL AND DEPOSITIONAL FEATURES OF EXPLOSIVE VOLCANIC DENSITY CURRENTS ON EARTH AND MARS

Abstract Approved: Redacted for privacy

Paul D. Komar

Straight, radial, erosional channels and fan-like deposits of tephra develop around steep-sided cones and composite volcanoes, but are not characteristic features of shield volcanoes. The channels and deposits normally are formed by explosive volcanic density currents which originate as nuées ardentes or base surges. The physical processes of explosive volcanic density current transport, erosion, and deposition are modeled using the equations developed to describe turbidity currents and grain flows, similar species of sediment gravity flows. The model predicts reasonable values for the flow densities and thicknesses of two photometrically timed nuée ardente eruptions, and illustrates that a nuée ardente probably develops from a single layer, highly mobile, autosuspended flow into a two layer system consisting of a high concentration, pseudo-laminar underflow and an over-

riding turbulent cloud. The model also makes possible quantitative comparisons between the driving forces of nuées ardentes, deep-sea turbidity currents, rivers and catastrophic floods such as that from Pleistocene Lake Missoula. These calculations indicate that the erosive potentials of nuées ardentes are far greater than river erosion but very similar to turbidity currents and catastrophic flooding.

A similar analysis for such flows on Mars shows that the velocities and driving forces compare with terrestrial nuées ardentes and base surges, but martian pyroclastic flows probably travel and disperse debris over greater distances. The presence of a permafrost terrain suggests the most plausible generating mechanism for explosive volcanic density currents in a martian environment is by hydromagmatic explosions. This mechanism may explain the steeper slopes, broad calderas, radial channels and blanketing flank deposits on a number of martian volcanoes (specifically Ceraunius Tholus, Uranius Tholus, Uranius Patera and Hecates Tholus) that were heretofore puzzling. Crater age data indicate these volcanoes probably represent an early to intermediate period of martian volcanism, on the order of 0.5 to 2 billion years older than the quietly erupted flank surfaces on the giant Tharsis shields and basal plains. These data are consistent with the view that martian atmospheric conditions in the past may have been more favorable for periodic burial of water and other volatiles in the vicinity of volcanic conduits, hence producing an extensive permafrost layer conducive to phreatic explosions and geothermal seepage. It also allows for explosive volcanism on a planet without moving plates.

THE FLOW MECHANICS AND RESULTING EROSIONAL AND DEPOSITIONAL FEATURES OF EXPLOSIVE VOLCANIC DENSITY CURRENTS ON EARTH AND MARS

by

Clare E. Reimers

A THESIS

submitted to

Oregon State University

in partial fulfillment of
the requirements for the
degree of

Master of Science

Completed July 1978

Commencement June 1979

APPROVED:

Redacted for privacy

Professor of Oceanography
in charge of major

Redacted for privacy

Dean of School of Oceanography

Redacted for privacy

Dean of Graduate School

Date thesis presented 10 July 1978

ACKNOWLEDGEMENTS

This study was suggested to me by my thesis advisor, Paul Komar. I would like to thank him for his contributions of scientific insight, personal encouragement, and one very long drive to Pasadena. I also owe thanks to Ken Scheidegger, Julius Dasch, and Pete Klingeman who acted as members of the thesis committee, and Karl R. Blasius of the Planetary Science Institute, Pasadena, California, who offered many helpful suggestions and provided access to the Viking imagery.

Drafting assistance was provided by Peggy Lorence and Sally Kulm. Cheryl Schurg helped with the typing.

This work was supported by the Planetology Program Office of NASA, grant NSG-7178.

TABLE OF CONTENTS

TABLE OF CONTENTS (continued)

LIST OF FIGURES

LIST OF FIGURES (continued)

LIST OF TABLES

PART I

THE NATURE OF NUÉES ARDENTES AND THEIR CLASSIFICATION

THE NATURE OF NUÉES ARDENTES AND THEIR CLASSIFICATION

INTRODUCTION

Explosive volcanic eruptions have always fascinated volcanologists, and descriptive accounts of their violence and destructiveness have flooded the geologic literature for nearly a century. Yet it is only within the last two decades that it has been appreciated that explosive volcanic density currents are also important agents for the transportation and deposition of tremendous volumes of fragmental debris.

The present study deals primarily with one type of explosive volcanic density current called a nuée ardente (glowing cloud), Figure 1. Other varieties which operate in a like manner include fissure erupted pyroclastic flows, lahars (volcanic mudflows), and volcanic base surges. The emphasis here is that these volcanic density flows are governed by the same mechanical forces as any other solid-fluid dispersion and hence, must create corresponding erosional and depositional features. For that reason, this first part of my study includes a discussion of ignimbrite deposition and channel erosion. The remainder of Part I is primarily a descriptive and historical account of nuées ardentes.

Parts II and III have been written as separate papers for publication. Part II extends the study of nuées ardentes and also base

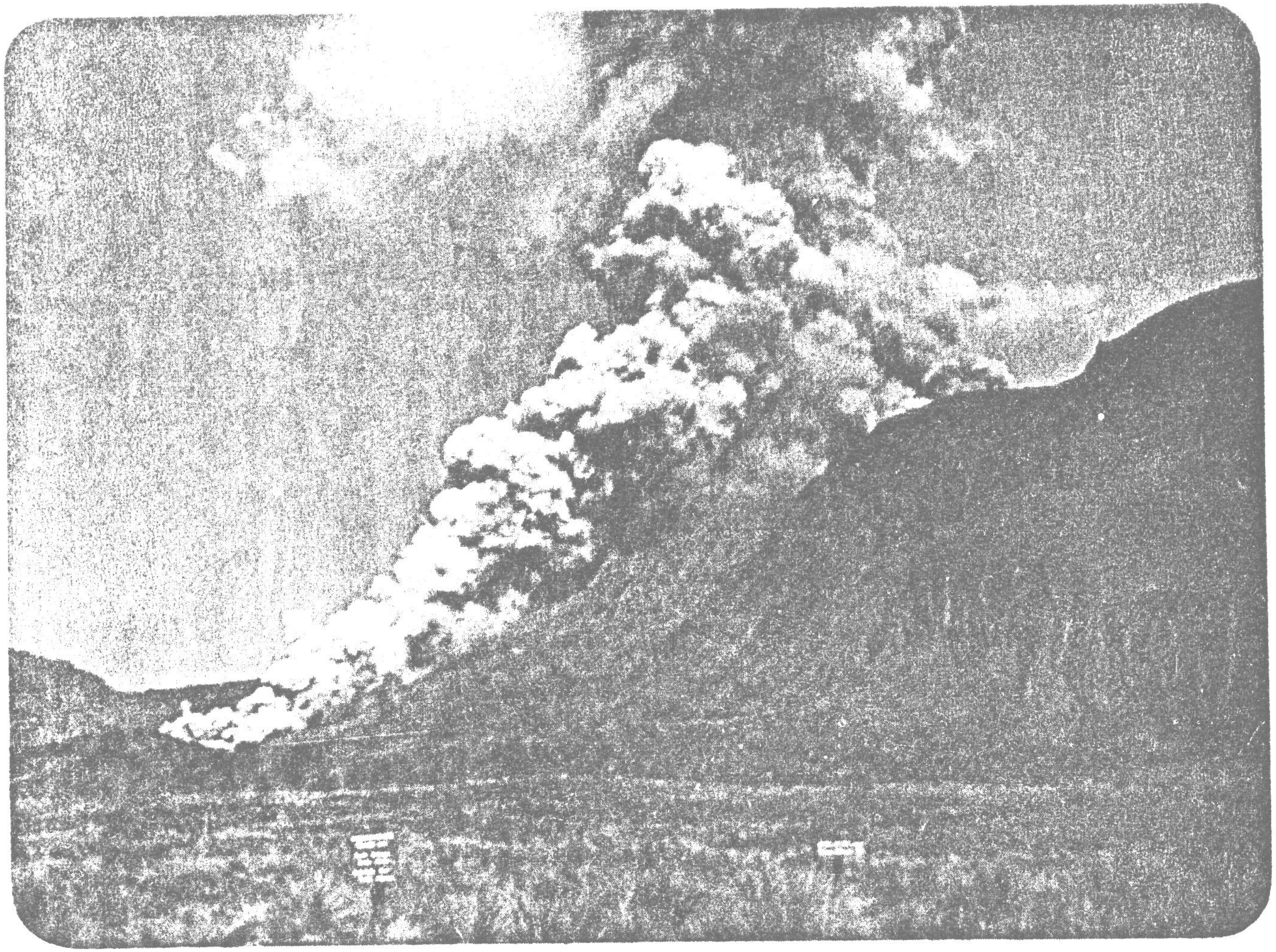

FIGURE 1: A nuée ardente

surges to the planet Mars. I suggest that there is evidence for the occurrence of explosive volcanic density currents on certain martian volcanoes, and that the frequency of these eruptions may be related to changes in martian climatic conditions.

Finally, Part III returns to the problem of nuée ardente physical properties and mechanics. Flow densities, thicknesses, and driving force terms are determined by a particle flux model for two photometrically recorded nuée ardente eruptions. These results are then applied to hypothetical flows on Mars.

THE NOMENCLATURE PROBLEM

To begin the analysis of the flow mechanics and resulting erosional and depositional features of nuées ardentes, it is necessary to identify just what is a "nuée ardente", because past definitions reviewed below, are ambiguous. The roots of the equivacacy becomes obvious if one traces the entire development of a nuée ardente. The main flow begins as a transient, highly turbulent, single layer surge which spreads laterally from the summit of a steep-sided volcano. The duration of this initial phase is usually only a few minutes and depends on modifying forces such as gravity, and on the size, temperature and trajectory of the generating eruption. From the surge develops a two layer flow consisting of (1) a low ground-hugging, fluidized avalanche, or underflow, and (2) an overriding, less dense, highly turbulent, billowing cloud or "ash hurricane" (Taylor, 1958), Figure 2. This two layer phase is followed by a rapid depositional phase which results

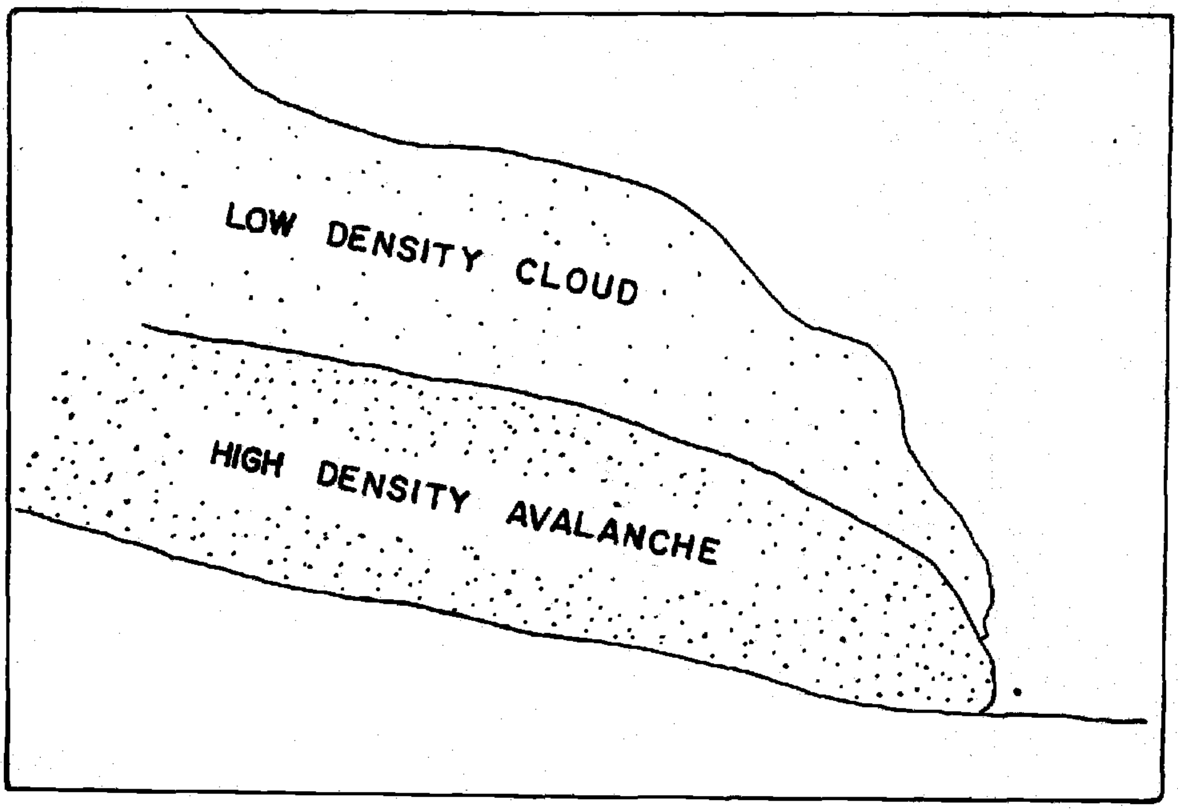

FIGURE 2: The divisions of a fully developed nuée ardente

when the driving force of the flow is no longer sufficient to maintain mobility. The majority of the deposits are emplaced in valleys several kilometers beyond the base of the source volcano.

Lacroix (1903) named these glowing eruptions of Mont Pelée after their conspicuous, but less massive overriding clouds of the second phase. Other accounts of nuée ardente eruptions emphasize the importance of the fiery avalanche (Anderson and Flett, 1903; Perret, 1935; Taylor, 1954, 1958; Aramaki, 1956; Macdonald and Alcaraz, 1956; Davis, Querry and Bonis, 1976, 1978), but few authors consider their entire development.

Another aspect of the nomenclature problem arises from the usage of the term "nuée ardente" to explain the eruption and emplacement of all pumice, scoria, block and ash flow deposits. For example, Aramaki (1957) defines a nuée ardente as equivalent to a pyroclastic flow in the "strict sense" but in order to explain the emplacement of different magnitudes of welded and non-welded deposits he proposes a three-fold classification based on differences in the magnitude of flows and the viscosity of the erupting magma.

TABLE I (from Aramaki, 1957)

Nuée Ardente in the strict sense	Pyroclastic Flow of the intermediate type	Pumice Flow

increasing magnitude →

decreasing viscosity →

In a later paper (Aramaki and Yamasaki, 1963), this classification is realized to be misleading and impractical and so abandoned. The authors instead propose that all types of flows composed of incandescent fragments be called pyroclastic flows, and that these should be classified by the bulk density and magnitude of their deposits which appear to relate to the eruptive stage of the source volcano.

Still other classification schemes exist in the literature, but because the widest-spread deposits (1000's km^2) have never been observed forming, there is little agreement as to what their parent eruptions should be called. MacGregor (1952, 1955) considers the nature of the source, the mode of initiation (explosive or nonexplosive), and the type of eruption as the most important diagnostic parameters for the distinction between different types of nuée ardente pyroclast eruptions. Table II is a listing of MacGregor's 1955 classification which also includes a description of the magma.

Williams (1957) simplifies MacGregor's classification into three main groups, namely, Peléan type directed explosions, Krakatoan type vertical explosions and avalanches, and fissure type upwellings of effervescing magma.

Smith (1960) does not recognize fissure eruptions as nuées ardentes. He suggests that the great welded-tuff sheets such as the Bishop's Tuff of southeastern California (which covers an area of 1000 square kilometers and locally is more than 150 meters thick) or the Yellowstone ignimbrite sheets (which cover 10,000 square kilometers and range from 150 to 300 meters thick) should be classified exclusively as fissure-erupted pyroclast deposits and not as a variety of nuée ardente deposit. Similarly, van Bemmelen (1963) refers to such voluminous pyroclastic flow deposits

TABLE II: An early classification of nuée ardente eruptions after MacGregor (1955)

Classification of nuée ardente eruptions

Nature of eruptions: Generalised description	Nature of eruptions: Major subdivisions	Mode of initiation	Source	Specific type of eruption	Magma	Volcano or locality name to link with specific type of eruption and magma	Description of eruptions as phases of complex eruptive sequences
Nuée ardente pyroclast eruptions: i. e. eruptions of gas and mobile, gas-generating (self-explosive) debris of new lava, accompanied by hot or glowing gas-and-dust clouds.	Tholoidal gas-and-avalanche eruptions*	Non-explosive	Summit-crater tholoid	Lateral disintegration type*	Trachytic	?	Gas-generating avalanche phases of tholoidal (andesitic) eruptive sequences.
					Rhyolitic	?	
					Andesitic*	Merapi	
			Tholoid on flank of volcano	Lateral disintegration type*	Andesitic*	?Santa Maria	
		Explosive	Summit-crater tholoid	Discharged lateral type**	Andesitic*	Mt. Pelée	
				Directed lateral type***	Andesitic*	Mt. Pelée	
				Vertically initiated type	Andesitic*	Mt. Pelée	
			Tholoid on flank of volcano	Discharged lateral type**	Andesitic*	Santa Maria	
				Directed lateral type***	Andesitic*	?Santa Maria	
				Vertically initiated type	Andesitic*	?	
	Non-tholoidal gas-and-ashflow eruptions**	Explosive	Summit crater	Vertically initiated type	Andesitic*	St. Vincent	Gas-generating ashflow phase of pyroclastic (andesitic) eruptive sequence
				Vertically initiated type	Rhyolitic	Mount Katmai	Gas-generating ashflow phases of pyroclastic (rhyolitic) eruptive sequences
			Low-level crater and (possibly) adjacent fissures	Vertically initiated type	Rhyolitic	Novarupta •	
			Many distributed fissures	Vertical, concealed fissure-orifice type	Rhyolitic	?	—

Major subdivisions: * Discharged debris comprises large or small blocks derived from the tholoid, as well as finely comminuted lava. ** Discharged debris is mainly finely comminuted lava.

Specific type of eruption: * No initial explosion. ** Mild initial explosion. *** Violent initial explosion.

Magma: * Including dacitic.

Volcano or locality: • Gas-generating ashflow phase of pre-tholoid (rhyolitic) eruptive sequence.

as "flood-tuffs", and he argues that they are the synorogenic acid counterpart of post-orogenic fissure-erupted "flood-basalts". Nuée ardente deposits, on the other hand, he states result from eruptions of normal volcanic cones with central vents.

The problem with these early classifications is that they fail to recognize three maxims of sedimentary fluid dynamics: (1) it is the physical properties of the flow (density, thickness, velocity, temperature) which govern how it erodes, transports and deposits debris; (2) these properties are subject to change dependent on the flow path (slope) and the duration of the flow; and (3) lithologically similar deposits may be formed by different initial (eruptive) mechanisms.

To clarify the nomenclature, the term nuée ardente will be restricted here to descriptions of an agent of transport of hot, gas-emitting, volcanic materials which generally develops into two parts: a basal avalanche, or underflow, and an overriding expanding cloud. Both portions of the nuée ardente must be generated from a normal volcanic cone and must be initially turbulent. A base surge is a volcanic density current very similar to a nuée ardente, but it must be generated by a phreatic eruption. The names pumice flow and ash flow will be used for acidic fissure erupted flows which may reach very high concentrations and be laminar in their movement. The term pyroclastic flow will be used as an inclusive term for the various mechanisms of dispersal of pyroclastic debris regardless of the source, and ignimbrite will refer to all of the various rock types produced by the emplacement of a pyroclastic flow (Fisher, 1966). These classifications are primarily genetic and intentionally do not specify flow magnitudes or the character of their deposits. This is because the physical properties of a flow which prevail during deposition determine the nature of the deposit. These final properties may not be the same as the properties that dominated the greater part of the duration of the flow, and may develop from different initial eruption mechanisms.

DESCRIPTIVE ACCOUNTS OF NUÉE ARDENTE FLOW

The earliest detailed description of a nuée ardente eruption is by T. Anderson and J.S. Fleet who on the evening of July 9, 1902 witnessed two nuées ardentes emerge from the summit of Mont Pelée. They wrote (1903, p. 504):

> The first cloud welled out quietly in the twilight, and was quite a small affair. It was black from the first - a foaming, boiling mass. Slowly it gathered speed, and came rushing along. The second was much larger, and in the darkness we could see that with it there was a glowing avalanche of red hot dust. It came down with far higher velocity, but, like the other, slowed down rapidly when it reached the sea ... Both were full of lightnings ....

Extreme mobility is characteristic of all nuées ardentes. In their account Anderson and Flett (1903) estimate that the July 9th avalanches may have reached velocities as high as 100 miles per hour (45 m/sec). They also observed that the velocities of these nuées ardentes changed along their course, the maximum velocities being reached on the mountain's lower slopes which are somewhat steeper than the cone.

For nuées ardentes changes in velocity are dependent on the gradient and the density difference between the mixture of gases and ash and the surrounding air. Gravity drives the mass, but unlike snow and rock avalanches the presence of gases:

> ... is essential; they are an original part of the mass, and without them there would be no flow. They are expanding, surging of their own inherent energy, and lift dust and sweep it along, while the dust in turn fetters them and compels them to keep to the surface of the ground (Anderson and Flett, 1903, p. 510).

The ground-hugging nature of the lower avalanche portion of the nuée ardente distinguishes and may even separate it from its overriding black cloud. On St. Vincent, a neighboring island to Martinique, Anderson and Flett (1903, p. 452) show that a nuée ardente avalanche from the island's Mont Soufrière clung to the valleys, turning almost at a right angle at one obstruction while the overlying cloud climbed the barrier and continued almost undeflected. At Volcan de Fuego, Guatemala, Davies et al. (1976) report that:

> Avalanches followed topographic lows, and where confined laterally by valley walls the conservation of momentum was high. Where the avalanches were able to spread out laterally they developed a surface morphology consisting of channels and levees. The largest grains were deposited in the channels.

Miller and Smith (1977) also demonstrate the ability of topography to channel the main mass of nuée ardente or ash flows by tracing flow deposits through valleys and over elevated passes of the Aleutian Range. They suggest that the general confinement of the flows to narrow valleys enabled a maintenance of velocities sufficient to overcome topographic barriers of more than 200 m high at distances of 20 to 40 km from the source. This agrees with the observation of Davies et al. (1976, 1978) that the flows from de Fuego did not loose momentum until emerging from the confines of valleys some 7 km from their source.

MODE OF GENERATION

At the source the role of gravity as the force directing the development and motion of a glowing avalanche is uncertain and may depend on the mode of eruption. Observations of nuées ardentes indicate that many are formed by an explosion of incandescent ash and blocks due to the release of gases confined with a lava mass. If the vent is not capped by a volcanic dome the initial ejection is directed vertically with subsequent downfalling and avalanching. This mode of generation produced the nuées ardentes on Soufrière as well as Mayon Volcano, Philippines (Moore and Melson, 1969) and St. Augustine Volcano, Alaska (Smith, Hobbs and Radke, 1977). The initial velocities of these flows are due predominantly to the conversion of potential energy to kinetic energy as the vertical eruption column falls back on the slopes, coalescing to form density currents. Wilson (1976) and Sparks and Wilson (1978) have modeled pyroclastic flows produced by column collapse, and they predict initial horizontal velocities up to 310 m/sec. Their values depend on the vent radius, gas content and vertical velocity of the blast which in turn control the height (potential energy). Subsequent velocities quickly become controlled by gravitational forces and retarding frictional drag and are rapidly reduced.

When the volcanic vent is capped by a dome, eruptions occur due to the build up of gases beneath the dome which cause it to burst at its weakest point. This is often near the base of the dome where cooling and fracturing has weakened the edifice (Macdonald, 1972). As a result the pyroclastic material is ejected horizontally at a low angle. Gorshkov (1963) distinguishes between "directed volcanic blasts" and vertical explosions. He argues that the two phenomena should not jointly be classified as nuées ardentes because they differ " in conditions of their expansion and the character of their deposition" (still another aspect of the nomenclature problem). It is true that in the proximity of the vent, deposits of directed blasts will have a greater percentage of blocks presumably derived from the shattered dome. In addition, the initial ejection of material laterally may give an added impulse to a developing avalanche. The avalanche, however, can not support large blocks for long and must quickly develop a quasi- equilibrium between the retarding frictional drag force and the driving gravity force component downslope. Thus, away from the immediate source, flow behavior is the same as for a vertical explosion, and both types of explosively generated avalanches are rightfully classified together. Examples of nuées ardentes generated by lateral explosions include the 1902 eruptions of Mont Pelée, Martinique (Lacroix, 1903; Anderson and Flett, 1903), Hibok-Hibok Volcano, Philippines (Macdonald and Alcaraz, 1956), and Bezymianny Volcano, Kamchatka (Gorshkov, 1959).

Still other types of generating mechanisms for glowing avalanches include the disintegration and collapse of a lava dome, or the avalanching of hot ash and lava which has accumulated on a steep slope (Moore and Melson, 1969; Macdonald, 1972). These types may behave more like a true rock avalanche showing less fluidity than those generated by explosion. The fluidity would depend upon the temperature and gas emission of the material, particle size, slope, and the amount of turbulence generated by the flow and the expanding gases within the mixture. Repeated collapse of the dome of Merapi Volcano, Java has produced a number of highly turbulent and mobile nuées ardentes (Aramaki, 1957).

THE ROLE OF GAS EMISSION AND AUTOSUSPENSION

In the initial stages of movement away from a volcano nuées ardentes will be highly turbulent, single layer flows with low particle concentrations. Many authors (Perret, 1935; MacGregor, 1952; Macdonald and Alcaraz, 1956; Taylor, 1958; and Macdonald, 1972) have proposed that gas emission during avalanching is the principal process responsible for maintaining turbulent flow and high mobility. However, McTaggart (1960) has demonstrated that high temperature flows can be highly mobile without gas emission. He observed that hot sands poured down an incline envelop air at their heads, the air then expands within the hot body of the flow creating turbulence. This process appears to be very similar to the entrainment of water by a turbidity current. Bagnold (1962) describes flows that are fluidized by turbulence created by entrainment as "autosuspended". The existence of basaltic nuées ardentes from Ulawun Volcano, New Britain (Melson et al., 1970) and Manam Volcano, New Guinea (Taylor, 1960) gives support to McTaggart's idea that the mobility of nuées ardentes is due to autosuspension caused by the steady inclusion and heating of air, with concomitant expansion. Basalts characteristically contain low contents of dissolved volatiles and hence could not emit large quantities of volcanic gases during avalanching (Melson et al., 1970). On the other side of the argument, the proponents of gas emission claim that blasts of cool air which precede many nuée ardente surges demonstrate that air is pushed out of the way of the flow. They point to avalanche deposits which often contain vesicular fragments with extensive vapor phase alteration (Ross and Smith, 1961) as evidence for gas emission. Tazieff (1969) also suggests that juvenile carbon dioxide makes the gas portion of a nuée ardente denser than the atmosphere, and thus partly explains its ground-hugging nature.

Perhaps it is reasonable that both gas emission and air entrainment are important processes for maintaining suspension of granular material and removing the yield strength of nuée ardente systems. The majority of nuées ardentes are derived from highly silicic magmas. For these Wilson (1976) and Sparks et al. (1978) have modeled the initial eruption column activity as a continuous jet of volcanic gases (primarily steam) which entrains air at its sides. Hence, after collapse the avalanche is already fluidized by both juvenile and atmospheric gases. In these early stages of flow the avalanche is also hottest and still internally explosive; later as the flow moves downslope juvenile volatiles would be replaced by air entrapped at the front of the moving avalanche or mixed across the upper interface of the flow. Thus in its final turbulent stages, a nuée ardente surge rushing down a steep slope would be fluidized primarily by entrapped air, regardless of the composition or volatile content of the erupting magma.

FLOW SEGREGATION AND DISPERSIVE PRESSURES

The ability of nuées ardentes to autosuspend particles by turbulence is dependent on a balance between the gravitational energy driving the flow and the energy lost due to friction. As long as this balance is maintained the particle concentration throughout the flow remains low and particle deposition takes place gradually by gravitational segregation of individual grains. This process builds a bed with distributional grading (Middleton, 1967).

However, previous descriptions indicate that a nuée ardente segregates into a two layer flow within distances of a few kilometers from the source. The basal portion has been suggested by Sparks et al. (1978) to have a high particle concentration formed by particle sizes which can no longer be supported by the turbulent gas phase. The upper dilute part is composed of gas and suspended fines. According to Bagnold (1954, 1956), at particle concentrations greater than about 9 percent by volume, grain-to-grain interactions within a suspension become significant resulting in an increase in apparent viscosity. As long as there is a sufficient driving force the suspension can remain fluidized without turbulence by dispersive pressures acting normal to the bed. Such dispersive pressures are greatest where the velocity gradient is maximum, and should vary as the square of the grain diameter for flows of cohesionless solids in which the effects of grain inertia outweigh those of the fluid's viscosity (Bagnold's inertial flow). However, if the driving force diminishes, the flow is emplaced "en mass" preserving its prior flow structure and particle distribution.

These theoretical considerations suggest that the flow of the high concentration basal avalanche portion of a nuée ardente should be governed in part by collisions between particles, that larger clasts should experience a greater net dispersive force away from the bed, and that evidence for these processes should be preserved in ignimbrites.

FLOW DURATION AND VOLUME: NUÉES ARDENTES VERSUS PUMICE FLOWS

Before emplacement the durations of nuées ardentes are restricted because they are produced by single short blasts or jets which are not capable of convective recovery (Sparks et al., 1978). A "long" nuée ardente eruption can last for hours or days, but most flows emerge, rush downslope, and dissipate in a matter of minutes. The volume of the deposits of such nuées ardentes rarely exceeds a few cubic kilometers and typically the deposits are a few tens of meters thick.

Large prehistoric fissure-erupted ash flows and pumice flows, if witnessed, probably could be distinguished in part from historic nuées ardentes by flow duration (and volume). Macdonald (1972) postulates that the ash flows responsible for the large rhyolite, dacite, and trachyte welded-tuff and ignimbrite sheets which cover areas of several thousand square kilometers in many parts of the world were generated by extreme frothing and gas-rich magmas which simply overflowed the lip of a vent, or multiple vents, with minor explosive activity. The duration of these outpourings must have taken days, weeks or even months, as successive eruptions rapidly followed an initial outburst in pulses of one great eruption (van Bemmelen, 1963). As a result, the volume and thickness of many prehistoric ignimbrites surpass that of nuées ardentes 10 to 100 times. Such compound units also more commonly contain thick zones of welding and exhibit deformation structures formed by the weight of the vertical column on slowly cooling pumice and lithic fragments.

THE NATURE OF IGNIMBRITES

Ignimbrite has been defined here as any deposit formed from a pyroclastic flow composed predominately of vesiculated volcanic material. Considerable discussion with regard to alternative generating mechanisms, variable flow durations, and the importance of outside forces such as gravity and bottom resistance on flow behavior and properties has also been presented. Consequently, it is important to emphasize that ignimbrites are as variable in composition and physical nature as the gas-particle flows from which they are emplaced.

Figure 3 depicts a "standard ignimbrite flow unit". The usual concept of a flow unit, as explained by Smith (1960), relates to the product of a single nuée ardente or pyroclastic flow. Units that result from the union of material from multiple vents are more complex. The terminology and field information summarized below is adopted primarily from Sparks and Walker (1973), Sparks et al. (1973), and Sparks (1976).

In the field the main portion of a single ignimbrite flow unit has two parts, a fine-grained basal layer (layer 2a), and a more massive, poorly sorted, overlying layer (layer 2b). The fundamental difference between layers 2a and 2b is that the former lacks coarse fragments (Sparks et al., 1973). In 2a both lithic and pumice clasts commonly show reverse grading up to a transitional contact with 2b. The lower boundary of the basal layer, which may separate it from the ground surface or layer 1, is usually sharp.

The thickness of layer 2a between contacts ranges from a few centimeters to > 1 m, and it may be welded. Layer 2b is several times thicker than 2a, usually unwelded, and poorly sorted. Examples of reverse grading of pumice clasts together with coarse-tail grading of lithic clasts are cited by Sparks et al. (1973) and Sparks (1976), but absence of grading or normal grading of pumice appear equally common (Smith, 1960; Fisher, 1966; Fisher and Mattinson, 1968; Sparks, 1976).

Ignimbrite layers 1 and 3 (Figure) are not invariably present, suggesting they represent subflows that originated from the main flow itself. Layer 3 is a thin, extremely fine-grained, bedded ash deposit

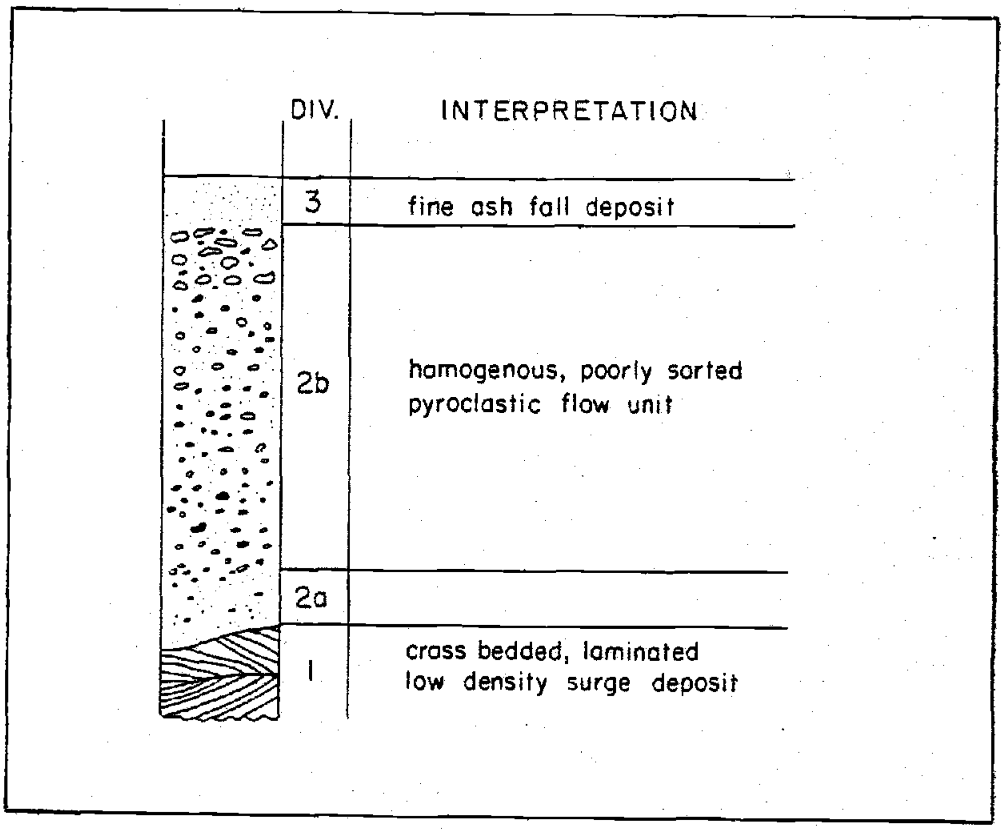

FIGURE 3: A standard ignimbrite flow unit after Sparks et al. (1973) and Sparks (1976)

which commonly shows an exponential decrease in thickness and grain size with increasing distance from the source. In comparison to layers 1, 2a, and 2b, layer 3 is depleted in crystals and lithic material.

Layer 1 is an extremely heterogeneous, well stratified, often cross-bedded deposit which generally only mantles a limited area proximal to the source. In fact, layer 1 deposits frequently occur without overlying layers on slopes greater than 10°. In thickness, layer 1 is seldom more than a few centimeters, and it often shows a pinch and swell structure. Grain size and sorting vary from one bed to another, but crystal and lithic material enrichment is common throughout.

INTERPRETATION OF IGNIMBRITE LAYERING

Layers 2a and 2b of an ignimbrite flow unit represent the primary end product of a nuée ardente avalanche. The poor sorting and inverse grading characteristic of these layers imply emplacement by rapid freezing of a high concentration suspension. Relative concentrations, however, must differ between individual flows in order to explain different degrees of grading in separate units.

The transition from layer 2a to 2b arises due to the exponential decrease in dispersive forces that mirrors the velocity gradient of a moving flow. Layer 2a represents an inertial regime where high shear and dispersive pressures effectively exclude large particles (Sparks et al., 1973). Dispersive pressures are not as strong in layer 2b, and there grading appears to be largely a function of buoyancy forces. The matrix of the flow is probably a mixture of volcanic dust and gases.

Particles that are less dense than the matrix of the flow have a positive buoyancy and tend to float. The larger the particle, the larger the buoyancy force, and the more effective the grading (Sparks, 1976). 2b layers where pumice fragments ($\rho_s \approx 1.0$ gm/cm^3) are reversely graded and lithic fragments ($\rho_s \approx 2.65$ g/cm^3) show coarse-tail grading must have had a flow matrix of intermediate density. This observation is important because it implies that indeed a low density nuée ardente is transformed to a high density flow prior to depositing its sediment load. It also gives some idea as to densities to be used in later models.

The grain size and blanketing nature of layer 3 indicates that it is an air-fall deposit and not an essential part of the ignimbrite. Recalling the dual nature of a nuée ardente, layer 3 is interpreted as stemming from the trailing billowing cloud portion and not the ground-hugging avalanche. Gravitational settling from the cloud produces normal grading and the lateral decrease in thickness and grain size of layer 3.

The occurrence of layer 1 has been interpreted by Sparks et al. (1973) as a "ground surge deposit" or by Sparks (1976) as a "pyroclastic surge deposit". According to Sparks, a surge differs from a pyroclastic flow in being highly turbulent and less dense. Pinch and swell structures, internal stratification and the sorting found in layer 1 support the view that it originates from a low concentration flow. Sparks and Walker (1973) postulate that ground surges are separate components of nuées ardentes which precede the main avalanche. Leading blasts of hot air, ash and sand have been reported for some nuée ardente eruptions (Anderson and Flett, 1903; Macdonald and Alcaraz, 1956; Gorshkov, 1959) which may be interpreted as "ground surges". It appears, however, that a more applicable explanation for the genesis of layer 1 is that it originates directly from the nuée ardente avalanche. Where the flow is still turbulent, autosuspension would prevent all but very dense lithic and crystal fragments from being deposited. This would explain the enrichment of these clasts in layer 1. The limited extent of layer 1 deposits and their occurrence on steep slopes without overlying layers also indicates deposition from an early and short lived stage of the nuée ardente. Where a complete sequence of layers exists, layer 1 probably represents the passage of the avalanche's head followed by a denser body which came to a rapid stop and "froze".

EROSIONAL FEATURES

The erosional features of nuées ardentes are not as well documented as the depositional features, probably because later flows, hot-rock slides and lavas tend to bury erosional features, or they become modified by rain and mud flows. Cotton (1944) attributes "parasol patterns of radial gashes and ribs" on Vesuvius and other growing cones to excavation by nuées ardentes. Clean swept and furrowed surfaces described by Perret (1935) also testify to the erosive power of the lower avalanching portion of a nuée ardente. If such a gouging process occurs leaving long deep gashes, later flows may be channeled by the depressions causing further scouring of the bottom. Successive nuées ardentes from the sharp cone of Merapi, Java have been observed to concentrate in avalanche gashes on the upper slope before fanning out on the lower slope (Cotton, 1944). Figure 4 shows nuées ardentes confined to ravines on the upper slope of Mayon Volcano, Philippines. Single channels and chutes, tens to hundreds of meters wide and up to several kilometers long, formed by a nuée ardente have also been reported (Asama Volcano, Aramaki, 1956; St. Augustine Volcano, Schmincke, personal communication, 1978). These will be described in greater detail in Part II.

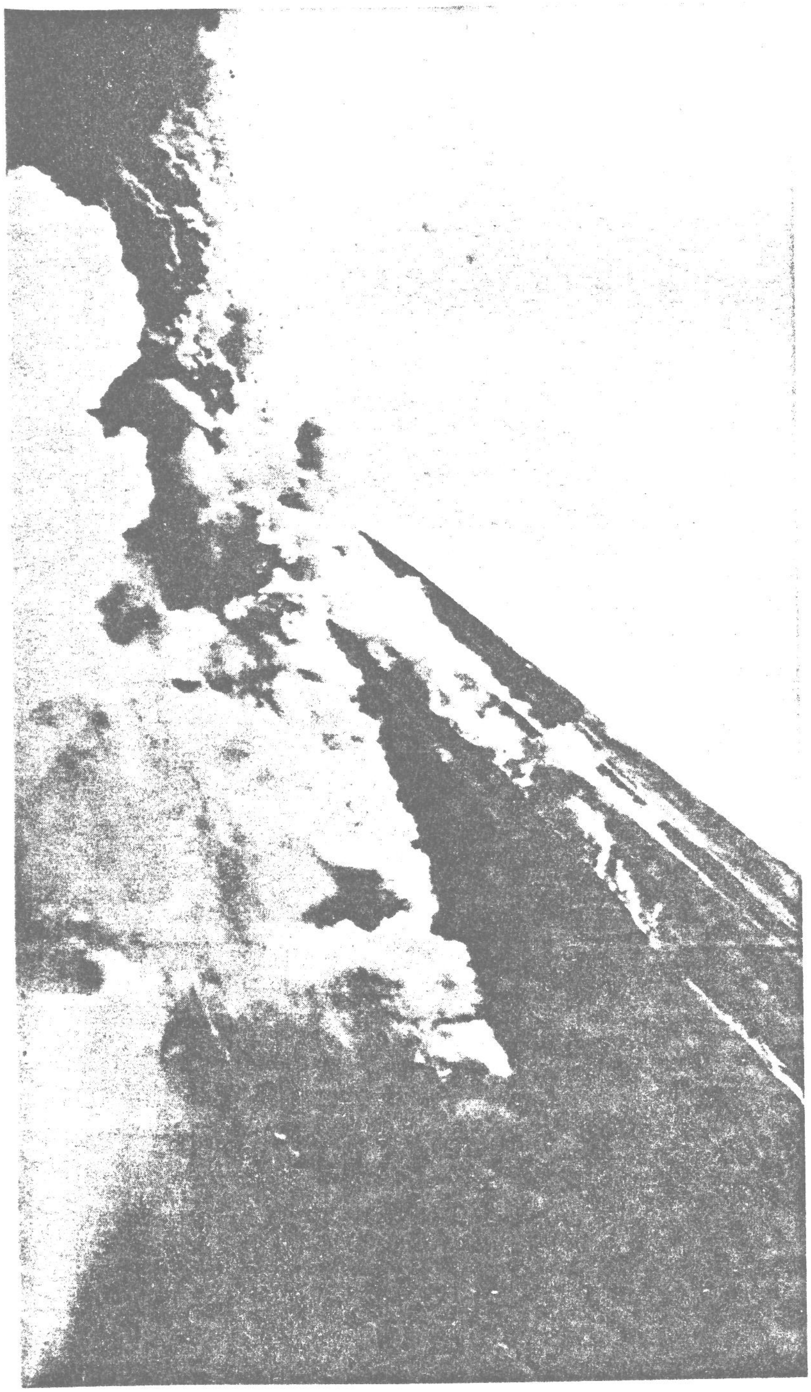

FIGURE 4: Nuées ardentes confined to ravines on the upper 500 meters of Mayon Volcano, Philippines on May 1, 1968. The picture is from Moore and Melson (1969).

REFERENCES

ANDERSON, T. & FLETT, J.S. (1903) Report on the eruptions of the Soufrière, in St. Vincent, 1902, and on a visit to Montagne Pelée, in Martinique. Phil. Trans. R. Soc. Lond., A 200, 353-553.

ARAMAKI, S. (1956) The 1783 activity of Asama Volcano. Parts I-II. Jap. J. Geol. Geogr. 27, 191-229, and 28, 11-32.

ARAMAKI, S. & YAMASAKI, M. (1963) Pyroclastic flows in Japan. Bull. Volcanol. 26, 89-99.

BAGNOLD, R.A. (1954) Experiments on a gravity-free dispersion of large solid spheres in a Newtonian fluid under shear. Proc. R. Soc. Lond., A 225, 49-63.

BAGNOLD, R.A. (1956) The flow of cohesionless grains in fluids. Phil. Trans. R. Soc. Lond., A 249, 235-297.

BAGNOLD, R.A. (1962) Auto-suspension of transported sediment; turbidity currents. Proc. R. Soc. Lond., A 265, 315-319.

BEMMELEN, R.W. van (1963) Volcanology and geology of ignimbrites in Indonesia, North Italy, and the U.S.A. Bull. Volcanol., 25, 151-173.

BOUMA, A.H. (1962) Sedimentology of some flysch deposits. A graphic approach to facies interpretation. Elsevier, Amsterdam, 168 pp.

COTTON, C.A. (1944) Volcanoes As Landscape Forms. Whitcombe & Tombs Ltd., London, 416 pp.

DAVIES, D.K., QUEARRY, M.W., & BONIS, S.B. (1976) Glowing avalanches, Volcan de Fuego 1974. EOS, 47, 346.

DAVIES, D.K., QUEARRY, M.W., & BONIS, S.B. (1978) Glowing avalanches from the 1974 eruption of the volcano Fuego, Guatemala. Bull. Geol. Soc. Am., 89, 369-384.

FISHER, R.V. (1966) Mechanism of deposition from pyroclastic flows. Am. J. Sci., 264, 350-363.

FISHER, R.V. (1971) Features of coarse-grained, high-concentration fluids and their deposits. J. Sedim. Petrol., 41, 916-927.

FISHER, R.V. (1977) Erosion by volcanic base-surge density currents: U-shaped channels. Bull. Geol. Soc. Am., 88, 1287-1297.

FISHER, R.V. & MATTINSON, J.M. (1968) Wheeler Gorge Turbidite-conglomerate series, California; inverse grading. J. Sedim. Petrol., 38, 1013-1023.

GORSHKOV, G.S. (1959) Gigantic eruption of the volcano Bezymianny. Bull. Volcanol. ser. 2, 20, 77-113.

GORSHKOV, G.S. (1963) Directed volcanic blasts. Bull. Volcanol. Ser. 2, 26, 83-88.

HOBBS, P.V., RADKE, L.F., & STITH, J.L. (1977) Eruptions of the St. Augustine Volcano airborne measurements and observations. Science, 4, 871-873.

KOMAR, P.D. (1972) Flow differentiation in igneous dikes and sills: profiles of velocity and phenocryst concentration. Bull. Geol. Soc. Am., 83, 3443-3448.

KOMAR, P.D. (1977) Computer simulation of turbidity current flow and study of deep-sea channels and fan sedimentation. In: The Sea: Ideas and Observations on Progress in the Study of the Seas, 6. (Ed. by E.D. Goldberg) Wiley & Sons, 603-621.

LACROIX, A. (1903) L'eruption de la montagne Pelée en janier 1903. Acad. Sci. (Paris) Comptes rendus, 136, 442-445.

MacDONALD, G.A. (1972) Volcanoes. Prentice-Hall Inc., Englewood Cliffs, New Jersey, 510 pp.

MacDONALD, G.A. & ALCARAZ, Z. (1956) Nuées ardentes of the 1948-1953 eruption of Hibok-Hibok. Bull. Volcanol. Ser. 2, 18, 169-178.

MacGREGOR, A.G. (1952) Eruptive mechanisms: Mt. Pelée, The Soufière of St. Vincent and the Valley of Ten Thousand Smokes. Bull. Volcanol. Ser. 2, 12, 49-74.

MacGREGOR, A.G. (1955) Classifications of nuée ardente eruptions. Bull. Volcanol. Ser. 2, 16, 7-10.

McTAGGART, K.C. (1960) The mobility of nuées ardentes. Am. J. Sci., 258, 369-382.

MELSON, W.G., JAROSEWICH, E. SWITZER, G., & THOMPSON, G. (1970) Basaltic nuées ardentes of the 1970 eruption of Ulawun Volcano, New Britain. Smithsonian Contr. to the Earth Sciences, 9, 15-32.

MIDDLETON, G.V. (1966-1967) Experiments on density and turbidity currents. Parts I-III. Can. J. Earth Sci. 3, 523-546, 627-637, and 4, 475-505.

MIDDLETON, G.V. & HAMPTON, M.A. (1976) Subaqueous sediment transport and deposition by sediment gravity flows. In: Marine Sediment Transport and Environmental Management. (Ed. by Stanley and Swift) Wiley & Sons, New York, 197-218.

MIDDLETON, G.V. & SOUTHARD, J.B. (1977) Sediment gravity flows. Chapter 8 in: Mechanics of Sediment Movement. SEPM Short Course, No. 3, Binghamton.

MILLER, T.P. & SMITH, R.L. (1977) Spectacular mobility of ash flows around Aniakchak and Fisher Calderas, Alaska. Geology, 5, 173-176.

MOORE, J.G. (1967) Base surge in recent volcanic eruptions. Bull. Volcanol., 30, 337-363.

MOORE, J.G. & MELSON, W.G. (1969) Nuées ardentes of the 1968 eruption of Mayon Volcano, Philippines. Bull. Volcanol., 33, 600-620.

PERRET, F.A. (1935) The eruption of Mt. Pelée 1929-1932. Carnegie Inst. Washington Publ., 458, 125 pp.

ROSS, C.S. & SMITH, R.L. (1961) Ash-flow tuffs: their origin, geologic relations and identification. U.S. Geol. Survey Prof. Paper 366, 81 pp.

SMITH, R.L. (1960) Ash flows. Bull. Geol. Soc. Am., 71, 795-842.

SOUTHARD, J.B. (1970) Impossibility of Bernoulli pressure forces on particles suspended in boundary layers: discussion of a paper by R.V. Fisher and J.M. Mattinson. J. Sedim. Petrol., 40, 518-519.

SPARKS, R.S.J. (1976) Grain size variations in ignimbrites and implications for the transport of pyroclastic flows. Sedimentology, 23, 147-188.

SPARKS, R.S.J., SELF, S. & WALKER, G.P.L. (1973) Products of ignimbrite eruption. Geology, 1, 115-118.

SPARKS, R.S.J. & WALKER, G.P.L. (1973) The ground surge deposit: a third type of pyroclastic rock. Nature Phy. Sci., 241, 62-64.

SPARKS, R.S.J., WILSON, L. & HULME, G. (1978) Theoretical modeling of the generation, movement, and emplacement of pyroclastic flows by column collapse. Jour. Geo. Res., 83, 1727-1739.

SMITH, J.L., HOBBS, P.V. & RADKE, L.F. (1977) Observations of a nuée ardente from St. Augustine Volcano. In press.

TAYLOR, G.A. (1958) The 1951 eruption of Mount Lamington. Bull. Bur. Miner. Resour. Geol. Geophys. Aust. 38.

TAYLOR, G.A. (1960) An experiment in volcanic prediction. Australian Bureau of Mineral Resources, Geology, and Geophysics, Record, 74.

TAZIEFF, H.K. (1969) Investigations of eruptive gases (abst). Intern. Assn. Volcanol. Chem. Earth's Interior, Sym. on Volcanoes and their Roots, Oxford Univ. Abst. Vol.

WALKER, G.P.L. (1971) Grain-size characteristics of pyroclastic deposits. Jour. of Geology, 79, 696-714.

WILSON, L. (1976) Explosive volcanic eruptions, III, Plinian eruption columns, Geophys. J. Roy. Astron. Soc., 45, 543-556.

PART II

EVIDENCE FOR EXPLOSIVE VOLCANIC DENSITY CURRENTS ON CERTAIN MARTIAN VOLCANOES

EVIDENCE FOR EXPLOSIVE VOLCANIC DENSITY CURRENTS ON CERTAIN MARTIAN VOLCANOES

CLARE E. REIMERS

School of Oceanography
Oregon State University, Corvallis 97331

ABSTRACT

A number of martian volcanoes, especially Ceraunius Tholus, Uranius Tholus, Uranius Patera and Hecates Tholus, show morphological features strikingly different from those of shield volcanoes but analogous to those of terrestrial cones and composite volcanoes such as Barcena Volcano, Mexico. The most distinguishing overall features are steep slope angles, and Krakatoa-type caldera morphologies. Erosional features comprise numerous radial channels which extend from below the rim toward the base of the dome, and in some cases, patterns of channels which emanate from small craters scattered on the flanks. Constructional features include blanketed flanks interpreted as dune or fan-like deposits of ash, and perhaps lava deltas. A possible explanation for the morphological features associated with these volcanoes is that they were formed by explosive volcanic density currents. Such eruptions would be expected on Mars where a rising magma came in contact with a thick layer of permafrost generating a base surge or after a Vulcanian explosion of a separate gas phase producing a nuée

ardente. In this analysis evidence is presented to attest that hydromagmatic explosions have taken place on Mars and that these are the planet's most significant generating mechanism for explosive volcanic density currents. If these interpretations are correct, crater age data from the surface of martian domes and shields indicate such phreatic activity occurred more frequently prior to 200 million years ago than in recent martian geologic history. This is consistent with the view that martian atmospheric conditions in the past were more favorable for cyclic release and burial of water and other volatiles in the vicinity of volcanic conduits. It also allows for explosive volcanism on a planet without moving plates.

INTRODUCTION

Mars has been recognized as a planet with a wide variety of volcanic features since the acquisition of Mariner 9 images. The most prominent volcanic constructs lie within the uplifted regions of Tharsis and Elysium (Figure 1). Ascraeus Mons, Pavonis Mons, Arsia Mons and Olympus Mons are the largest examples of martian volcanism and occur within Tharsis (Table I). Each is a gently sloping shield volcano with a summit caldera and surface features indicative of construction by successive eruption and accumulation of low viscosity basaltic lavas (Carr, 1973, 1975; Carr et al., 1977; Greeley, 1973).

A fifth giant volcano is Elysium Mons. Owing to its steeper slopes (averaging 10-12°), blanketed flanks, and the presence of numerous apparently endogenic craters within its caldera and on its

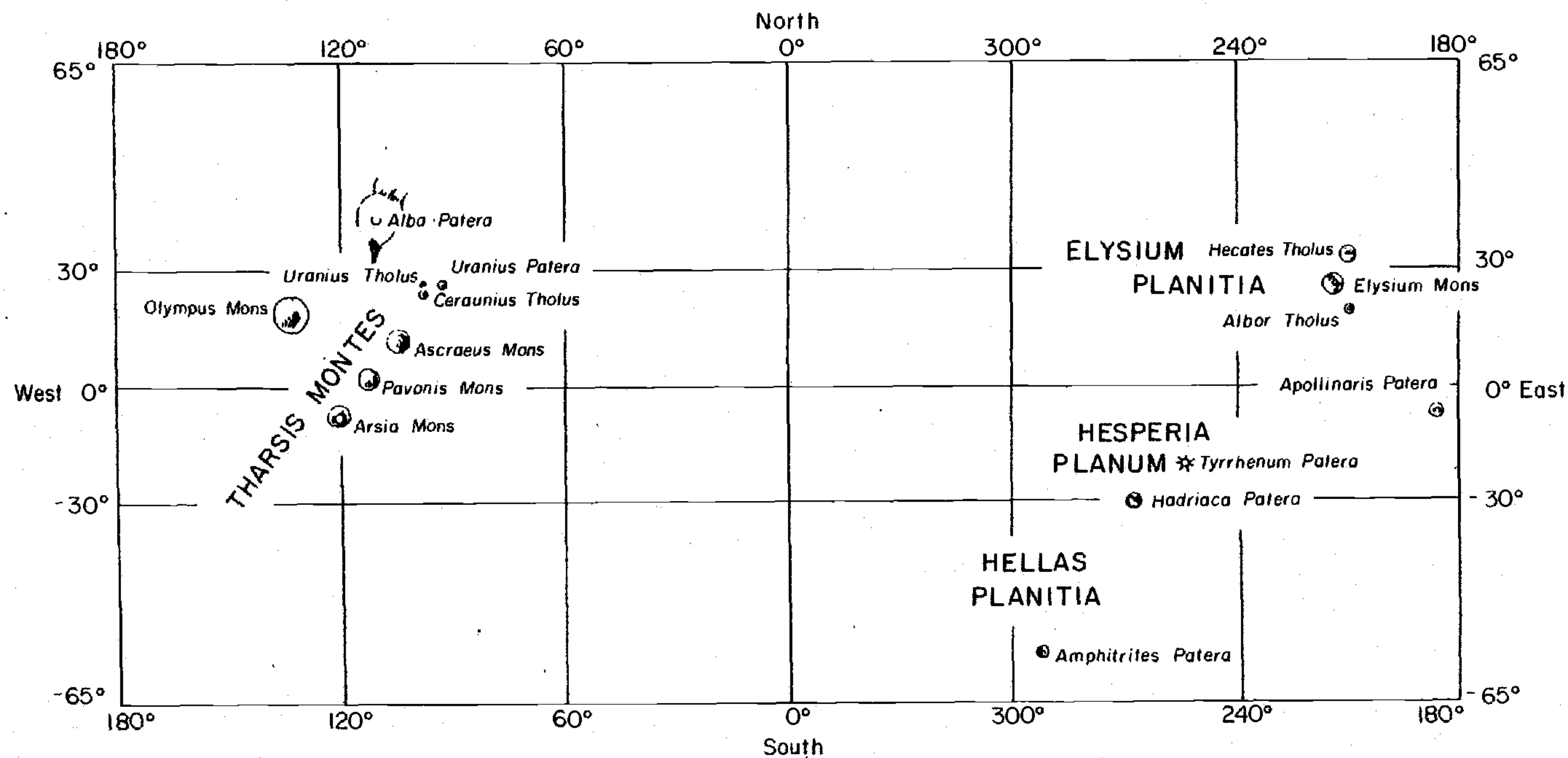

FIGURE 1: Map showing the location of the most prominent volcanic constructs on Mars.

TABLE I: Summary of the characteristics of the principal Martian volcanoes. Age data is from Carr (1975).

VOLCANO	REGION	HEIGHT ABOVE PLAINS (km)	DIAMETER (km)	AVERAGE SLOPE	AGE (millions of years)	DESCRIPTION	CLOSEST TERRESTRIAL COUNTERPART
OLYMPUS MONS (Carr, 1975; Carr et al., 1977)	THARSIS	23 ± 3	500 - 600	5^o - 6^o	200	Shield has a complex caldera approximately 80 km across. Its terraced flanks are radially textured by well-defined leveed flows, ridges and collapse pits. Around much of its margin is an escarpment up to 6 km high.	HAWAIIAN SHIELDS
ASCRAEUS MONS (Carr, 1975)	THARSIS	19 ± 3	400	5^o - 6^o	400	Shield has several overlapping summit calderas; the largest is approximately 50 km across. Terraced flanks show numerous small pits and merge smoothly with the surrounding plains. The northeast and southwest margins are intersected by swarms of irregular cracks.	HAWAIIAN SHIELDS
PAVONIS MONS (Carr, 1975)	THARSIS	19 ± 3	400	5^o - 6^o	400	This volcano has a single central caldera roughly 40 km across. Its flanks are similar to Ascraeus Mons except for numerous concentric grabens which extend from the caldera to the outmost flanks.	HAWAIIAN SHIELDS
ARSIA MONS (Carr, 1975; Carr et al., 1977)	THARSIS	19 ± 3	400	5^o - 6^o	800	Resembles Pavonis Mons. Caldera is about 80 km in diameter. Elongate lava flows appear to originate at a reentrant in the edifice and spred out onto the surrounding plains.	HAWAIIAN SHIELDS
CERAUNIUS THOLUS	THARSIS	10 ± 1	100 - 130	10^o - 12^o	500 - 1,000	Dome-shaped volcano has a circular 12 km-diameter crater with a flat floor. Northwest crater rim is breached by a network of channels, the largest of which connects with an impact crater at the volcano's base. Numerous finer channels radiate down the steep evenly textured slopes from below the crater rim.	BARCENA VOLCANO, MEXICO
URANIUS THOLUS	THARSIS	3 ±.5	55 - 65	5^o - 6^o	500 - 1,000	Resembles Ceraunius Tholus except it has a double crater which is breached at two points. The inner crater is 8 km across; the outer is 15 km across.	TAAL VOLCANO, PHILIPPINES
URANIUS PATERA	THARSIS	UNKNOWN	300	UNKNOWN	500 - 1,000	Abroad central caldera approximately 150 km across dominates this construct. Its slopes are evenly textured and relatively featureless.	—
ELYSIUM MONS (Malin, 1977)	ELYSIUM	14 ± 1.5	170	10^o - 12^o	1,000 - 2,000	This topographically asymmetric volcano has a single central caldera about 14 km across, and roughly textured, heavily cratered slopes. Large channel-like forms emanate from the caldera.	EMI KOUSSI, TIBESTI
HECATES THOLUS (Malin, 1977)	ELYSIUM	6 ± 1	180	3^o - 5^o	1,000 - 2,000	Dome-like volcano with a convex profile, and 12 km-diameter complex caldera. Flanks have a hummocky texture and are heavily cratered. Numerous radial channels extend in a parallel pattern down the slopes. Other channels emanate from craters on the lower flanks.	ULAWUN VOLCANO, NEW BRITIAN
ALBOR THOLUS (Malin, 1977)	ELYSIUM	3 ±.5	130	2^o - 3^o	1,000 - 2,000	Multiple central caldera about 30 km across is surrounded by roughly textured slopes and a series of grabens. Resembles Tharsis shields more than other Elysium volcanoes.	HAWAIIAN SHIELDS
ALBA PATERA (Carr et al., 1977)	—	6 ± 2	1,600	$<1^o$	1,000 - 2,000	A ring of fractures about 600 km across surrounds a poorly defined central caldera complex. Numerous flow features are traceable for more than 1000 km from the central vent.	—
APOLLINARIS PATERA	—	12 ± 2	135 - 175	8^o - 10^o	2,000 - 3,500	This volcano has a broad circular caldera about 85 km across. Its flanks are heavily cratered but show a pattern of radial depressions which extend from below the rim across what appears to be thick deposits of fine material.	BARCENA VOLCANO, MEXICO (?)
HADRIACA PATERA	HELLAS	2	200 - 260	$<1^o$	3,500 - 4,000	Central featureless area 70 km across is surrounded by radial ridges, depressions and channels.	—
AMPHITRITES PATERA	HELLAS	1	400 - 450	$<1^o$	3,500 - 4,000	Highly degraded volcanic structure with central caldera roughly 100 km across, and a radiating structure of ridges and valleys.	—
TYRRHENUM PATERA (Carr, 1975)	HESPERIA	UNKNOWN	500	$<1^o$	3,500 - 4,000	Sometimes called "Dandelion", it has radiating depressions around a central disc.	—

flanks, Malin (1977) suggests that Elysium Mons is a composite volcano significantly different from the Tharsis shields. Generally, terrestrial composite or stratovolcanoes are formed by the intercalation of lavas and pyroclastics. These represent the mixed products of alternating effusive and explosive character eruptions. It may, therefore, mean that sometime in its history Elysium Mons exhibited large scale explosive activity.

In this paper a number of other martian volcanic constructs will be studied which display morphological features suggestive of explosive volcanism. At the northeast margin of Tharsis are clustered three volcanic domes, Ceraunius Tholus, Uranius Tholus, and Uranius Patera. A similar dome, Hecates Tholus, is located in north Elysium (Figure 1). Important differences between these smaller domes and the Tharsis shields include: (1) slope angles, (2) caldera morphologies, (3) the presence on the domes but not on the shields of numerous radial channels which extend as deep but discontinuous incisions from just below the rim toward the base of the cone, and (4) apparent blanketing deposits (ash?) on the lower flanks of the domes but not on the shields.

A possible explanation for the morphological features associated with the domes is that they were formed by explosive volcanic density currents. On Earth such eruptions are of two types; base surges generated by magma coming in contact with water or water-soaked rock, and nuées ardentes produced by explosive exsolution of juvenile gases during rapid extrusion of large volumes of oversaturated magma (Moore, 1967). Both flows have been observed to originate from characteristic sources and to produce diagnostic erosional and depositional features which are not found on shield volcanoes. The initial focus of this paper, therefore, will be to establish the nature of explosive volcanic density currents, discuss their associated landforms, and compare their erosional and depositional features in order to determine possible martian counterparts. Specific corroborating evidence from the 1952 hydromagmatic eruption of Barcena Volcano, Mexico will be presented because this terrestrial volcano shows surface features similar to those of Ceraunius Tholus (though at differing scales), an observation which may have profound implications for the development of the martian volcano. Finally, two speculative topics will be considered: (1) explosive volcanism on a planet without moving plates, and (2) evidence for copious ground water and climatic change early in martian history.

EXPLOSIVE VOLCANIC DENSITY CURRENTS AND VOLCANIC LANDFORMS

Base Surges. A base surge is a turbulent ring-shaped cloud formed by expanding gases at the base of a vertical eruption column (Moore, 1967). On Earth volcanic base surges have been observed to arise from shallow phreatic eruptions, but the term also applies to density flows produced by events such as hypervelocity impacts and nuclear explosions. As pointed out by Moore (1967) base surges travel at high velocities (20-42 m/sec), but they may form without a downslope gradient. They also do not require high temperatures or any specific radial component from an initial blast to maintain mobility.

Volcanic base surges are typically laden with a diverse mixture of steam, mud and coarse ejecta. Most of this load is acquired during strong initial explosions which blast large amounts of debris upward within a central eruption column. Potential energy is converted to kinetic energy as the column falls back on the slopes, coalescing to form density currents which then spread radially, dispersing debris by flow and fallout (Fisher and Waters, 1970; Waters and Fisher, 1971; Schmincke et al., 1973).

Descriptions of base surge bedforms and erosional features show them to be common in the rim deposits of a class of small volcanoes called maars (Moore, 1967; Fisher and Waters, 1969; Heiken, 1971; Fisher, 1977). In general, maars are volcanic landforms built by the continuous or episodic ejection of hyaloclastic debris around a volcanic vent. The vent may occur in association with other volcanic features or may stand alone.

The first three columns of Table II compares the characteristics of tuff rings and tuff cones (true maars) with related cinder cones. Tuff rings are small volcanoes characterized by broad saucer-shaped craters and a low ejecta ring (Macdonald, 1967, 1972; Heiken, 1971). Hyaloclastic ash of basaltic composition commonly constitutes the major component of the ejecta, but more acidic ashes also have been found. Typical examples of tuff rings occur in the Christmas Lake Valley Basin, South Central Oregon (Heiken, 1971). There water from a paleo-lake apparently came in contact with rising magmas creating

TABLE II: Comparison of major volcanic constructs on Earth.
Typical profiles. (A) Hole in the Ground Crater, Oregon; (B) Diamond Head, Hawaii; (C) Lassen Park, California; (D) Mayon Volcano, Philippines; (E) Mauna Loa, Hawaii. From Macdonald (1967, 1972) and Heiken (1971).

CONSTRUCT	TUFF RING	TUFF CONE	CINDER CONE	COMPOSITE VOLCANO	SHIELD
TYPICAL PROFILE					
AVERAGE SLOPE	4^0- 12^0	10^0-13^0	7^0- 22^0	10^0- 35^0	2^0- 12^0
SUMMIT MORPHOLOGY	broad saucer-shaped crater	broad saucer-shaped crater	small bowl-shaped crater with irregular rim	funnel-shaped opening as the result of explosions, or bowl-shaped depression as the result of collapse	large sunken caldera or multiple calderas; often rim is breached due to lava flows or faulting
LITHOLOGY	sideromelane tuff, lapilli tuff and tuff breccia; possibly some cinders and basalt flows; abundant accretionary lapilli	sideromelane tuff, lapilli tuff and tuff breccia; possibly some cinders and basalt flows at summit; accretionary lapilli	tachylite cinders; flows of holocrystalline basalt; traces of sideromelane ash	interbedded lava flows and layers of ash and cinders	base consists of wide spreading flows of tholeiitic basalt; commonly towards the end of the life of the volcano, lavas change to alkali basalts, mugeavite,hawaiite, and trachyte; summit maybe capped by spatter or cinder cones
SEDIMENTARY STRUCTURES	parallel radiating channels; dunes and fan-like deposits	parallel radiating channels; well defined graded beds; dunes and fan-like deposits	poorly defined thick beds; slump features	block lava flows; nuee ardente channels and deposits; mudflows	pahoehoe and aa flows; lava tubes and channels; concentric or radial fissures and dikes; fault scarps
STYLES OF ERUPTION AND MODIFICATION	airfall and base surge clouds generated by contact of rising magma with water at shallow depths; slumping	airfall and base surge clouds generated by contact of rising magma with water at great depths; slumping	airfall and slumping of ejecta generated by explosive release of juvenile or non-magmatic gases	Strombolian, Volcanian or Peleean eruptions usually from central pipe vent; some eruptions occur from lateral vents; rain generated streams and mudflows	effusive central and lateral vent eruptions of Hawaiian or Strombolian type; faulting; minor hydromagmatic explosions

subaqueous debris flows, base surges, and showers of ejecta. Similar eruptions have formed tuff rings where rising magma encountered ocean water, ground water, or melt water from ground ice or snow (Moore, 1967; Fisher and Waters, 1969).

Tuff cones differ from tuff rings principally in shape and geologic cross section. The shapes of these features appear to depend on the depth of explosion, the amount of water available to generate steam, and the type of surrounding material (Moore, 1967; Heiken, 1971; Fisher and Waters, 1970). Tuff rings with gentle slopes are common features of shallow eruptions of magma in contact with abundant ground or surface water in non-volcanic strata. In contrast, steeper tuff cones more commonly arise from explosions deep within volcanic strata where water is less accessible. In essence, the morphological difference between tuff rings and tuff cones reflects the radial distance attained by base surges formed at the vent. First the outward expansion of a base surge is increased after a shallow eruption because some of the explosion energy is vented horizontally giving an added impulse to the density flow. Secondly, if abundant water is present, steam will continue to feed the flow as long as fresh magma is rising within the conduit. Finally, less energy is required to disaggregate and transport loose nonvolcanic alluvium than is required for a dense volcanic strata such as basalt. Thus, base surges generated at shallow depths by the contact of abundant water with a magma rising through a low density stratum will probably result in a wider spread of ejecta and steam, creating tuff rings with low profiles, rather than tuff cones.

Cinder cones constitute a third volcanic landform associated with explosive ejection of pyroclastic debris. Cinder cones are not true maars because sufficient water is seldom available in the vicinity of a cinder cone to create high velocity base surge flows associated with tuff rings and tuff cones. Instead, the principal depositional mechanism is air-fall which may build the cinder cone to the angle of repose of the disaggregated debris. The craters of cinder cones are commonly small and bowl-shaped. The rim may be irregular owing to breaching by succeeding explosions or slumping. A typical cinder cone with an average slope of about 8° was formed within the explosion crater of Lake Taal, Volcano Island, Philippines, after a phase of phreatic eruptions in 1965 (Moore et al., 1966). Apparently, the source of water was cut off from the vent near the end of the eruption, altering the character of the eruption. Again the availability of water at volcanic vents is an important controlling factor for subsequent volcanism.

<u>Nuées Ardentes</u>. A nuée ardente ("glowing cloud") is best characterized as a type of volcanic density current with two parts: (1) a hot, normally incandescent, highly mobile, ground-hugging avalanche, and (2) a hot, turbulent, expanding, ash-laden cloud which is derived from the avalanche but may become separated and extend beyond the terminus of the avalanche (Lacroix, 1904; Smith, 1960; Moore and Melson, 1967; Melson et al., 1970). Nuées ardentes form from the explosive release of magmatic gases within a superheated, oversaturated with vola-

tiles, lava mass. Normally, the lava has an acidic to intermediate rock composition, but basaltic nuées ardentes have been reported from New Guinea and New Britain Islands (Taylor, 1960; Melson et al., 1970). The diversity of magmas associated with nuées ardentes may be explained by Verhoogen's (1951) suggestion that the conditions which favor over-saturation and explosive ash formation depend more on the kinetics of the erupting process than on the original viscosity and gas content of the magma. That is, a rapidly rising magma, rich in crystals, should be explosive regardless of composition.

As documented by timed photography the initial velocity of a nuée ardente may excede 50 m/sec (Moore and Melson, 1968; Stith et al., 1977). Momentum is imparted to the flow by its source explosion, by the hydrostatic pressure difference between its head and surrounding fluid (air), and by the pull of gravity where movement is downslope. Further, it appears that where confined to ravines on the upper slopes of a volcano, the flow mechanics of a nuée ardente are similar to those of a turbidity current. That is, initially the main avalanche portion of the nuée ardente may be treated as a solid-fluid dispersion which nearly exhibits Newtonian behavior. Sediment is supported within the fluid phase by turbulence which is generated by the kinetic energy of the flow (Bagnold's "autosuspension", 1962), and these factors result in high shear stress on the surface beneath the flow. On the gentle lower flanks of a volcano or where movement is uphill, energy is rapidly lost, however, and a nuée ardente avalanche no longer behaves like a turbidity current but develops into a high concentration, non-turbulent pyroclastic flow, or underflow (Davies et al., 1978), similar to a debris flow. Indirect evidence for this transformation is suggested by the common characteristics of poor sorting and reverse grading seen in most ignimbrites and debris flow deposits.

Another generality with regards to nuées ardentes is that they tend to originate from lava trapped beneath domes or within the conduits of steep-sided composite volcanoes. Composite volcanoes constitute a major category of volcanic edifice characterized by symmetrical profiles and complex structures of interbedded layers of tephra and lava flows. Table II compares composite volcanoes with both the volcanic forms discussed in association with base surges, and shield volcanoes. Although shields are not commonly recognized as the source of any form of explosive volcanic density current, they are included because they constitute the most prominent volcanic construct heretofore studied on Mars.

CRATERS, CHANNELS AND DUNES FORMED BY EXPLOSIVE VOLCANIC DENSITY CURRENTS

In addition to the general profiles and structures outlined in the previous section, certain morphological features distinguish volcanoes that have had a quiet effusive history from those that have had an explosive history. Breached, noncircular, sunken, summit calderas or multiple craters, rift zones, partly collapsed lava tubes and lava flow channels are characteristic of shield volcanoes; broad circular explosion craters, radial channels, and thick dune-like deposits of surface debris are characteristic of tuff rings and cones. Composite volcanoes commonly show a mixture of both categories of crater and flank features (Table II).

Eruptions from the summits of most shield volcanoes produce individual flows of fluid lavas which generally breach the crater rim. Once on the flanks, flows tend to be narrow and may build a variety of constructional features. Greeley (1971, 1973) and Greeley and Hyde (1972) describe the formation of lava channels and tubes. They suggest lava channels can be identified morphologically by a simple form penecontemporaneous with the surrounding terrain, distributary branching, and the development of levees or topographic ridges along the axis of the channel. Discontinuous parts of a flow channel represent sections that were roofed to form lava tubes. Carr (1974) and Cutts and Blasius (1977) have also suggested that under conditions of sustained flow, high eruption temperatures, and low yield temperatures lava channels may form by means of thermal incision and/or mechanical plucking. Evidence for lava erosion on Earth includes "cut banks" and overhangs at meander bends in several tubes described by Greeley (1971) and Greeley and Hyde (1972), and inclusions of country rock in lava flows. However, no predominantly erosional lava channel has ever been observed on Earth, and the eruption rates and durations required by thermal models may limit channel formation by lava erosion to examples which show evidence of re-cut terraces, truncated surface features, and large lava deposits at the mouth of the lava channel.

Channels formed by explosive volcanic density currents are erosional rather than constructional. Nuées ardentes characteristically cut large channels tens to thousands of meters wide (Aramaki, 1956; Moore and Melson, 1969; Fisher, 1977); an example is shown in Figure 2. The channels originate on the steep upper flanks of composite volcanoes, where the avalanche portion of the nuée ardente flows rapidly and the shear stress is high. Further downslope they are replaced or filled by thick deposits of volcanic debris which are emplaced "en mass" by the avalanche and/or by fallout from the cloud. Nuée ardente channels may develop radially when influenced by pre-existing drainage [Mayon Volcano, Philippines (Moore and Melson, 1969)], or as new single features [Asama Volcano, Japan (Aramaki, 1959); St. Augustine Volcano, Alaska (Schmincke, pers. comm., 1978)].

Base surges are also known to erode radiating channels, but these generally are U-shaped and only a few meters to tens of meters wide. Table III compares the dimensions of channels cut by terrestrial volcanic density currents. A distinguishing characteristic of base surge channels is that they do not breach the crater rim but originate on the upper flanks where the base surges develop. Away from the crater rim the channels may widen and follow pre-existing topographic lows. In many instances the channels are abruptly replaced by dunes and fan-like deposits at the base of the volcano. The dunes and fans are base surge deposits which may extend several kilometers from the eruption center. Field studies by Fisher and Waters (1970), Schmincke et al. (1973), and Matterson and Alvarez (1973) indicate that individual bed

FIGURE 2: Channel carved by the 1976 St. Augustine Volcano Nuée Ardente. The channel is approximately 100 meters wide and 10 meters deep. The photograph was received from H.U. Schmincke (Institute fur Mineralogie, Bochum, W. Germany).

TABLE III: Comparison of channels cut by explosive volcanic density currents on Earth.

LOCATION	AGENT(S)	AVERAGE SLOPE*	WIDTH (m)	DEPTH (m)	WIDTH/DEPTH	LENGTH (m)	COMMENTS
BARCENA VOLCANO (Richards, 1959; Moore, 1967)	BASE SURGES	7^{o}-8^{o}	3 - 7	1 - 3	3 - 2.3	up to 430	straight, U-shaped, non-coalescent channels; issue from below the crater rim; terminate beyond slope break under a blanket of dune-like tephra deposits
KOKO CRATER, HAWAII (Fisher,1977)	BASE SURGES STREAMS	11^{o}- 12^{o}	.4 - 5.5	.1 - 3	4 - 1	——	U-shaped prehistoric channels in a bedded tuff; some base surges followed pre-existing stream channels
LATERA CRATER, ITALY (Matterson and Alvarez,1973)	BASE SURGES	——	4 - 30	2 - 15	2	——	U-shaped prehistoric channels; intiate below collapsed crater in region of maar volcanoes
TABLE ROCK, OREGON (Heiken,1971)	BASE SURGES	4^{o} - 12^{o}	2 - 30	1 - 21	4 - 2	——	U-shaped radial channels; begin below crater rim and extend to massive tuff deposits; tuff rings and tuff cones
ST AUGUSTINE VOLCANO, ALASKA (Fisher,1977; Schmincke, pers. comm.)	NUEE ARDENTE	12^{o}	100	10	10	"several hundred"	between the crater and main depositional fan a single deep erosional channel was cut in older clastic deposits; other channels formed on the fan itself; composite volcano
MAYON VOLCANO, PHILIPPINES (Moore and Melson,1969)	NUEES ARDENTES	21^{o}	50 - 300	5 - 15	20 - 10	>500	radial straight ravines; modified by rains; composite volcano
ASAMA VOLCANO, JAPAN (Aramaki, 1956)	NUEE ARDENTE	14^{o}	1100 - 2000	up to 40	50	>8000	single box-shaped channel cut along the upper course of nuee ardente; channel is replaced by area of deposition along lower course; immediately after the nuee a lava flow partially filled the channel; composite volcano

* This represents an average for the entire flank of the volcano. The channels often are found only on the steeper upper slopes.

waves are developed across the deposits with long axes approximately perpendicular to the current direction. Wave lengths of tens to a few meters progressively decrease outward, reflecting the deceleration and loss of competence of the currents with distance from the eruption center. The total area of deposition may include tens to hundreds of square kilometers.

A specific example of the development of radial channels leading to lower flank dunes is provided by the 1952 base surge eruption of Barcena Volcano, Mexico. This terrestrial volcano may represent an instructive counterpart to many of the martian domes, especially Ceraunius Tholus, and so its history is summarized in the following section.

MORPHOLOGY AND DEVELOPMENT OF BARCENA VOLCANO

Barcena Volcano is a large tuff cone situated at the southern end of Isla San Benedicto, Islas Revillagigedo, Mexico (Figure 3). Barcena, 340 meters above sea level, was born by explosive eruption between August 1, 1952 and February 28, 1953. No subsequent activity has occurred (Richards, 1959; Endrodi, 1975).

San Benedicto is located on a 75 kilometer wide, 3.5 kilometer high, north-south trending volcanic ridge that intersects the Clarion Fracture Zone at 19°18'S, 110°48'W. The ridge is part of a submarine mountain range extending south from San Benedicto to Clipperton Island. The rocks of San Benedicto are primarily alkali-calcic tuffs with lavas younger than similar rocks dated from the other Revillagigedo Islands to the west (Richards, 1959, 1966). Various aspects of the geology and geochemistry of the Revillagigedo Islands have been discussed by Richards (1959, 1966), Bryan (1966, 1967) and Endrodi (1975).

Barcena Volcano is classified as a tuff cone because of its 7°-8° slopes, its crater and flank morphology, and its constructional history (Table II). According to Richards' (1959) summary of the 1952-1953 eruption, the growth of the cone was initiated by two days (August 1 and 2, 1952) of phreatomagmatic explosions which expelled more than 200 million cubic meters of tephra. These eruptions were presumed by Richards (1959) and Moore (1967) to have arisen from the volatilization of ground water in the porous, ashy strata of Monticulo Cineritico, a pre-eruption, eroded, pyroclastic cone. Towering eruption columns and radiating base surges accompanied the blasts, spread tephra, and built the cone.

By mid-August the most violent eruptions had ceased, but small intermittent base surges or "tephra avalanches" (Richards, 1959) continued until mid-September, 1952. These density flows descended from below the crater rim and eroded furrows in the unconsolidated tephra (Figure 4). On the steep upper flanks of the cone the furrows were straight and U-shaped, 3 to 7 meters wide, 1 to 3 meters deep, and an average of 240 to 270 meters long. Below the slope break the furrows widened, became irregular and finally disappeared under a blanket of dune-like tephra deposits. Similar instances of base surge channel formation and deposition has been inferred from rim bedforms of volcanoes located in Eastern Oregon (Heiken, 1971), Italy (Matterson and Alvarez, 1972) and Laacher See, Germany (Schmincke et al., 1973).

FIGURE 3: Aerial view of Barcena Volcano, Isla San Benedicto, Islas Revillagigedo, Mexico. Delta Lavico is to the lower left. To the upper right is an old crater which was partially obliterated during the eruption of Barcena. The picture is from Richards (1959).

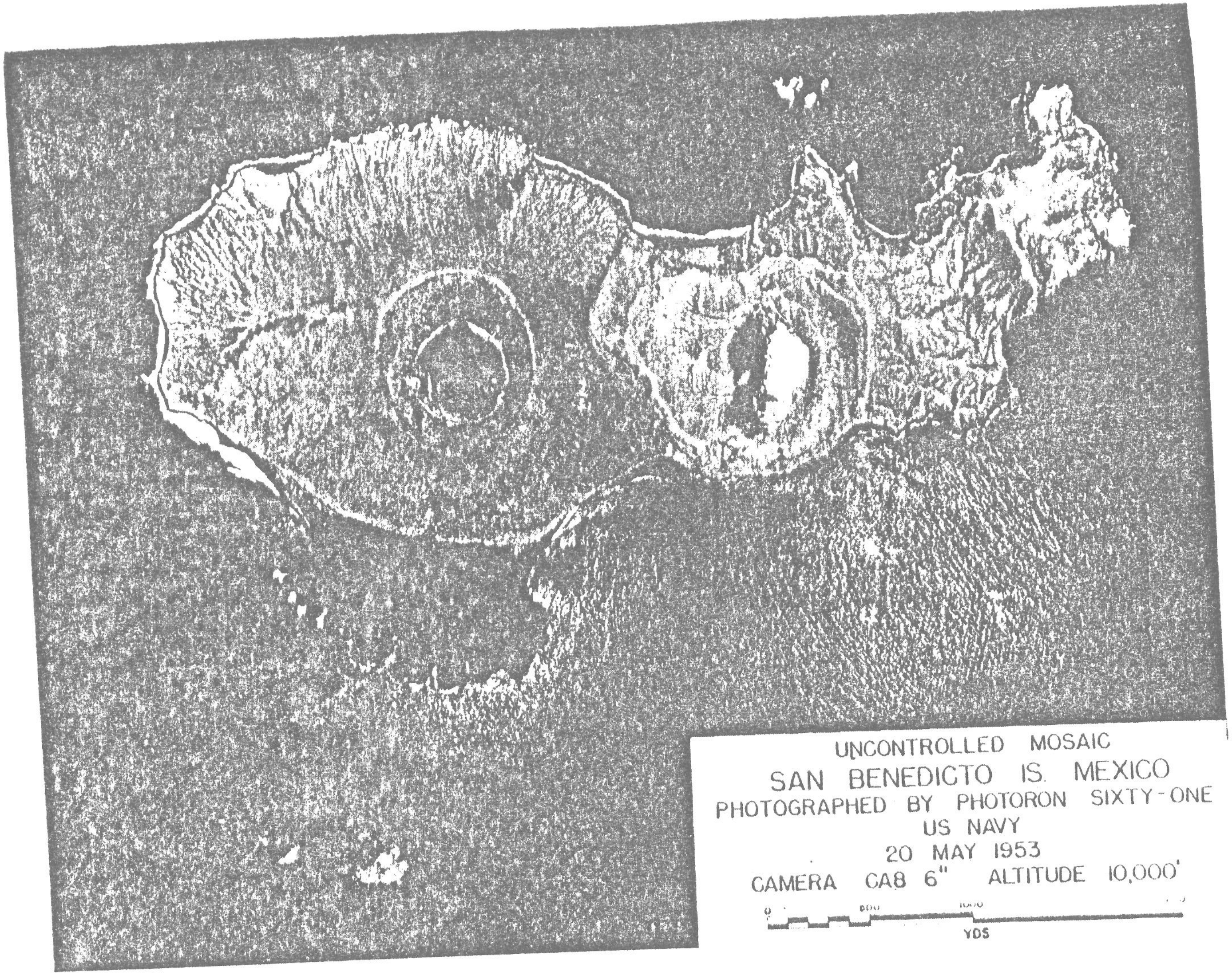
UNCONTROLLED MOSAIC
SAN BENEDICTO IS. MEXICO
PHOTOGRAPHED BY PHOTORON SIXTY-ONE
US NAVY
20 MAY 1953
CAMERA CA8 6" ALTITUDE 10,000'
YDS

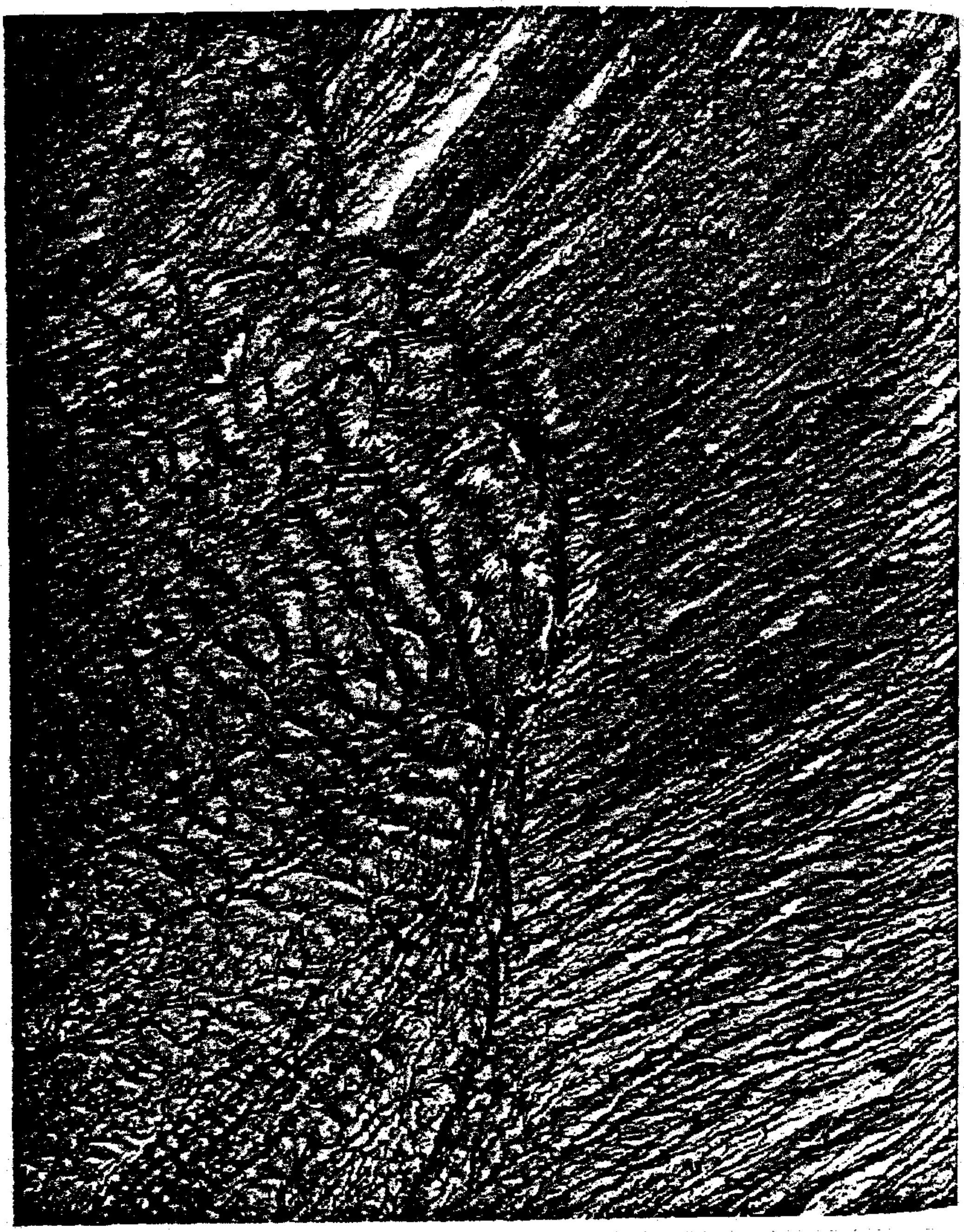

FIGURE 4: Photograph showing channels eroded by base surges on Barcena Volcano. Above the slope change the channels are about 3-7 meters wide, 1-3 meters deep, straight and parallel. Below the slope change the channels tend to coalesce and terminate in an area of deposition. The picture is from Richards (1959).

During the explosive phase of the eruption of Barcena Volcano no lava could be seen in the explosion crater, and the crater was bowl-shaped with a pronounced regular rim. A small dome on the crater floor capped the magma conduit. Renewed activity in November and December 1952 partly filled the crater with viscous lava, formed a second dome, and deposited ash on the lee side of the crater. On December 8, a landslide originated on the southeastern seacliff of Barcena. Later that day the slide area became the source of a lava flow which spread out into the sea forming a broad deltaic feature (Figure 3). This feature remained active until late February 1953 and has since been named Delta Lavico (lava delta). Above Delta Lavico the crater rim was faulted with 4-5 meter vertical displacement. If volcanism should resume at Barcena, it is likely that lava would breach the crater at this point.

MARTIAN VOLCANISM AND VOLCANIC MORPHOLOGIES

The idea that explosive volcanism has occurred on Mars is not new. West (1974) has described a number of small martian cones that may be related to pyroclastic activity; King and Riehle (1974) have proposed that the origin of the basal scarp fringing Olympus Mons is most probably by erosion of ash flow tuffs which presumably were deposited by nuées ardentes; and Malin (1977) has suggested that Elysium Mons is most likely a composite volcano with numerous endogenic craters and associated ash deposits. He also describes Hecates Tholus as a highly evolved feature, much like a terrestrial tholoid, only extremely larger.

Less prolific, but related, theories of explosive volcanism have been proposed to explain a number of features associated with lunar maria. The most relevant lunar-terrestrial analog is the suggestion by Cameron (1964) that Schroter's Valley and other lunar sinuous rilles which have a crater at one end owe their origin to the erosive agency of nuées ardentes. He cites Aramaki's (1956) description of the channel cut during the 1783 eruption of Asama Volcano, Japan as supporting evidence (Table III). Fisher (1969) has proposed similar arguments to explain the origin of extensive areas of lunar "patterned ground". He suggests these areas are probably undulating dunelike features deposited by lunar base surges. The major difference between the morphologies of the lunar features described by Cameron and Fisher and their terrestrial counterparts is in scale. The lunar features, like the martian examples, are much larger.

The focus of the remainder of this paper will be primarily upon the question of the role of explosive volcanism in the origin and development of the four martian domes mentioned in the introduction, Hecates Tholus, Ceraunius Tholus, Uranius Tholus and Uranius Patera. As indicated by Malin's (1977) comparative analysis of Hecates Tholus, these four domes and other martian volcanoes may exhibit certain common surface features which distinguish them from shield volcanoes. Accordingly, the following discussion will describe newly photographed flank and caldera features of the four martian volcanoes, and compare their features with possible terrestrial counterparts. From these identifications, some attempt will be made to interpret the styles of eruption that were responsible for the construction of the martian domes.

Hecates Tholus. The Elysium province of Mars contains three volcanoes which lie in a triangular pattern on the crest of a broad regional dome (Figure 1). The northernmost volcano, Hecates Tholus (Figure 5), has a 12 km-diameter, complex caldera, rises about 6 km above the surrounding plains, and is approximately 180 km in diameter (Malin, 1977). The history of Hecates Tholus is difficult to interpret, but a good possibility is that it was formed by a variety of eruption types which produced viscous lavas intermittently with ash. At the time of this writing the Viking coverage of Hecates Tholus is incomplete. On revolution 86, Viking orbiter 1 acquired a set of high resolution frames of the volcano's northern terminus and fringing plains. Moderate resolution Mariner 9B-frames show the complete region and have been described by Malin (1977).

The Viking photographs reveal numerous $\leq$ 1 km-wide channels and at least four 4 to 10 km-diameter craters on the lower flanks of Hecates Tholus (Figure 6). Most of the larger channels appear to follow the hummocky topography and must originate near the summit. Generally, these channels are without levees, and do not coalesce. Many exhibit significant breaks in continuity beginning as deep channels which shallow markedly only to deepen and continue a few km further on. On

FIGURE 5: Photomosaic of Mariner 9B-frames showing Hecates Tholus (DAS No's. 13496368; and 13496298). Flow channels breach the rim of the complex caldera and radiate downslope. The upper flanks have a hummocky topography and are heavily cratered. The lower flanks have a smoother topography. The large embayment in upper center may be a secondary caldera or an eroded impact crater.

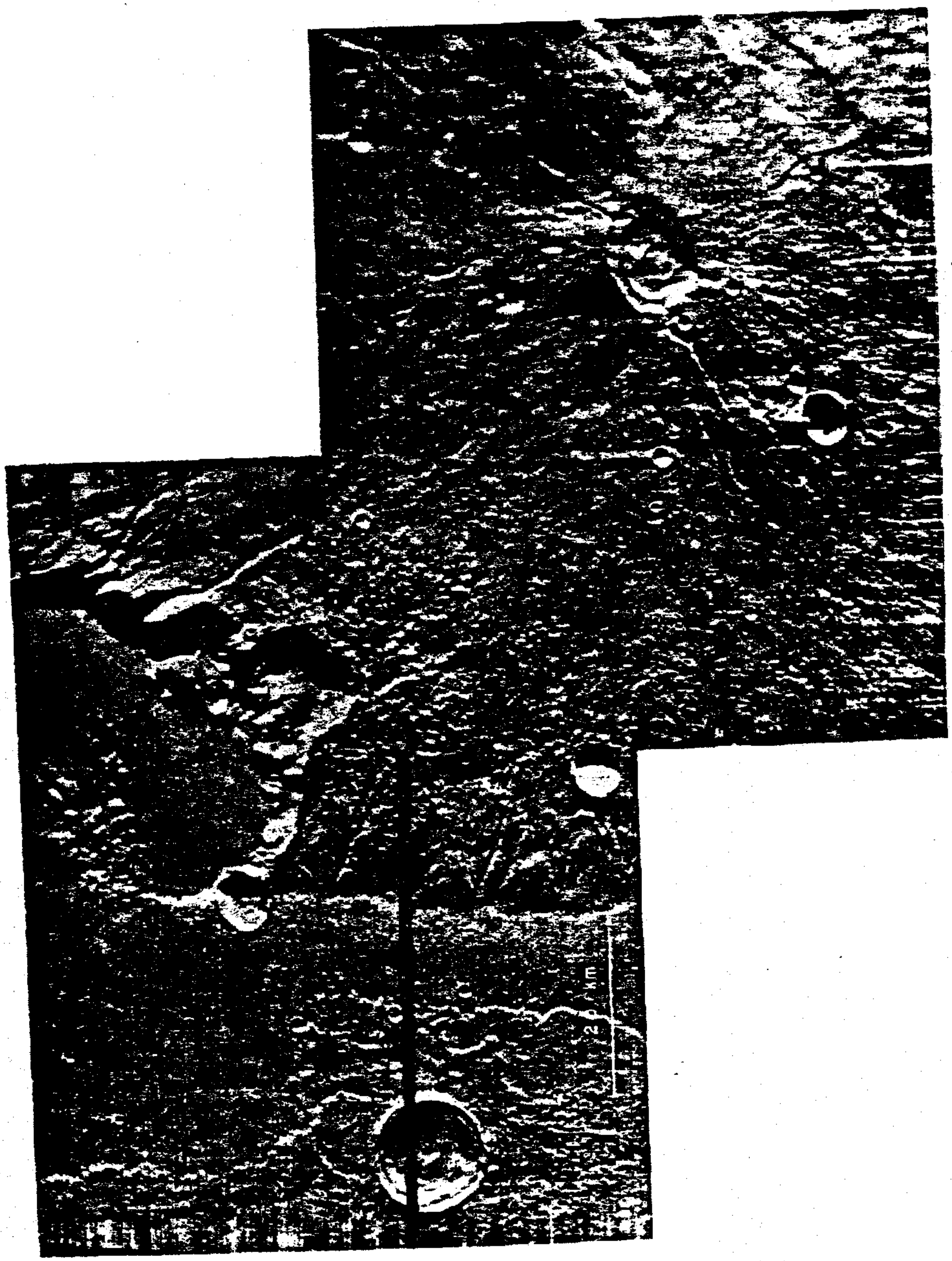
20 km

FIGURE 6: Viking mosaic (No. 211-5274) of part of the lower flanks of Hecates Tholus and surrounding plains. Two types of channels are visible. The first originate near the summit and follow topographic contours downslope in a radial pattern. The second emanate from flank craters. Both sets of channels are without levees and probably erosional. The collapsed plains to the upper center may have resulted from the removal of ground ice.

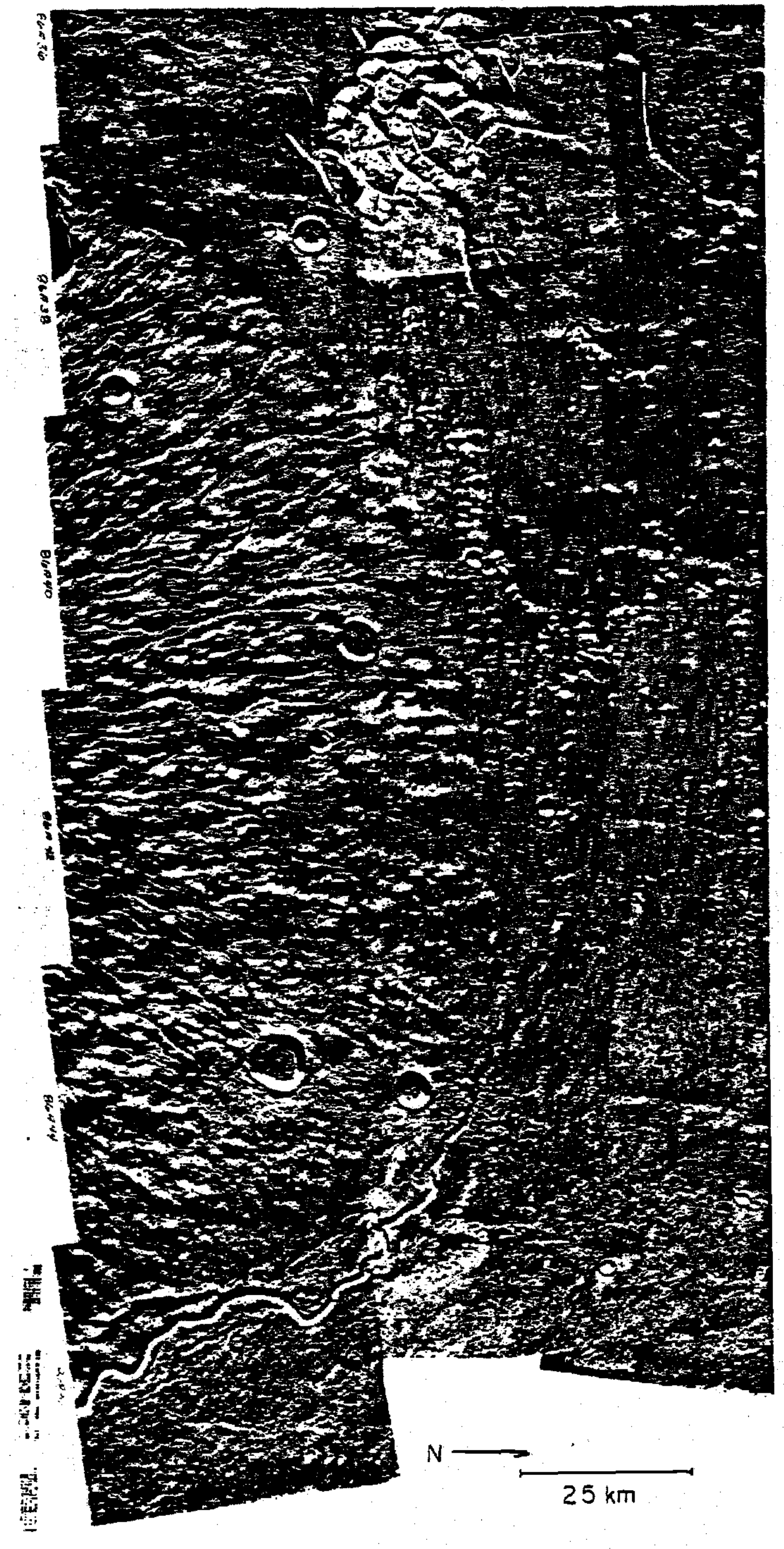
N
25 km

the upper flanks the distribution density of channels is greatest in part due to numerous small channels that contribute to the main channels as systems of fine criscrossing tributaries. Towards the terminus of the flanks, most of the channels abruptly end, and the slope is contoured by more rolling hummocks spaced by distances ≳ 6 km. This more subdued topography may represent wind modified fan-like tephra deposits similar to ash beds at the bases of many terrestrial tuff cones and composite volcanoes.

A different set of channels seem to emanate from two of the five largest flank craters (the smallest and the largest). These and two other flank craters appear superposed onto slope channels. The second largest crater has an ellipitical depression (a meteoritic crater?) upslope. The rimmed bowl-shaped morphologies of these craters suggest they were formed by explosive events. On Iceland eruptions from Katla Volcano have been wholly explosive, although the volcano is fed by a deep-seated basaltic magma like most shield volcanoes. Thorarinsson (1967) has suggested the explosive activity of Katla is entirely due to external conditions, explicitly covering ice and a pervious ground. If a permafrost layer occurs within porous ashy materials on the lower flanks of a martian volcano, magma rising into ice-filled fractures should give rise to shallow phreatic explosions, creating flank craters much as in Iceland. Secondly, if the ground water could be mobilized and mixed with magmas within the central conduit, large hydromagmatic explosions might lead to the formation of Plinian eruptions and base surge density flows at the summit. These flows would be expected to erode deep non-coalescing channels in unconsolidated tephra deposits but would be less effective over more resistant surfaces. Finally, hydrothermal activity could supply water to the summit in the form of seeps. In places, the seepage could form tributaries to feed and modify the already existing base surge channels. Such a seepage process is not unlike the mechanism of particle extrusion and sapping presumed to be responsible for the dissection of sinuous radial gullies with convergent courses on the New Guinea volcano, Vulcan (Ollier and Brown, 1971), and , combined with explosive volcanic density current erosion , is preferred to alternative suggestions that the martian channels were eroded by lava flows. Lava erosion requires extremely high temperature, fluid lavas and sustained flow (Carr, 1974; Cutts and Blasius, 1977). The subdued hummocky topography of Hecates Tholus suggests it has been frequented by the eruption of highly viscous lavas and blanketing ash (Malin, 1977). Sustained lava flow should erode relatively uniform, regularly sinuous channels and deposit vast lava fields at the mouths of the debouching channels. The Hecates Tholus slope channels are irregularly sinuous, U- and V-shaped and vary considerably in both width and depth. In addition, there are no apparent volcanic flow forms around the northern boundary of the volcano. Instead, partially collapsed or "chaotic terrain to the northwest of Hecates Tholus (Figure 6) suggests the presence of extensive ground ice in this area of Elysium (Carr and Schaber, 1977). If this interpretation is correct, it indicates that conditions may have existed condusive to the production of highly erosive base surge density currents, hydrothermal seeps, and phreatic flank explosions.

Uranius Tholus, Uranius Patera, and Ceraunius Tholus. Perhaps the best examples of martian volcanic constructs that differ from shield volcanoes are the three volcanic mountains which are clustered at the northeast margin of the Tharsis region of Mars (Figure 1). A swath of pictures acquired on orbits 229 and 516, by Viking Orbiter 1, and on orbit 38, by Viking Orbiter 2, show a surprising diversity of shape and surface features among the three volcanoes (Figure 7). Uranius Patera is nearly 300 km in diameter and is the broadest volcano in the group. The name Patera (meaning saucer) reflects the size and shape of its central caldera which is about 150 km across and flat floored. Numerous craters larger than 1 km in diameter also pock the caldera floor. The caldera may be essentially a Krakatoa type caldera which formed as follows: First, after a period of voluminous explosive eruptions of magma as pumice falls and pumice flows, the summit probably collapsed. Second, a period of activity followed which filled the caldera with lava. The lava then solidified forming the flat floor. Finally, the craters within the caldera wall indicate the volcano entered a period of repose which has only been interrupted sporatically by relatively small explosion events triggered by either meteoritic impact or phreatic mixing.

One puzzling aspect of the Viking pictures of Uranius Patera is

FIGURE 7: View of the northeast margin of the Tharsis region of Mars as seen by the Viking orbiters. Ceraunius Tholus is situated near the bottom of the picture. A channel network heads at the broken northwest rim of its circular summit caldera. Above Ceraunius Tholus is Uranius Tholus. Both domes exhibit numerous fine channels which radiate from near the summit over evenly textured flanks. The large sucer-shaped caldera to the right is Uranius Patera (Mosaic No. 211-5593).

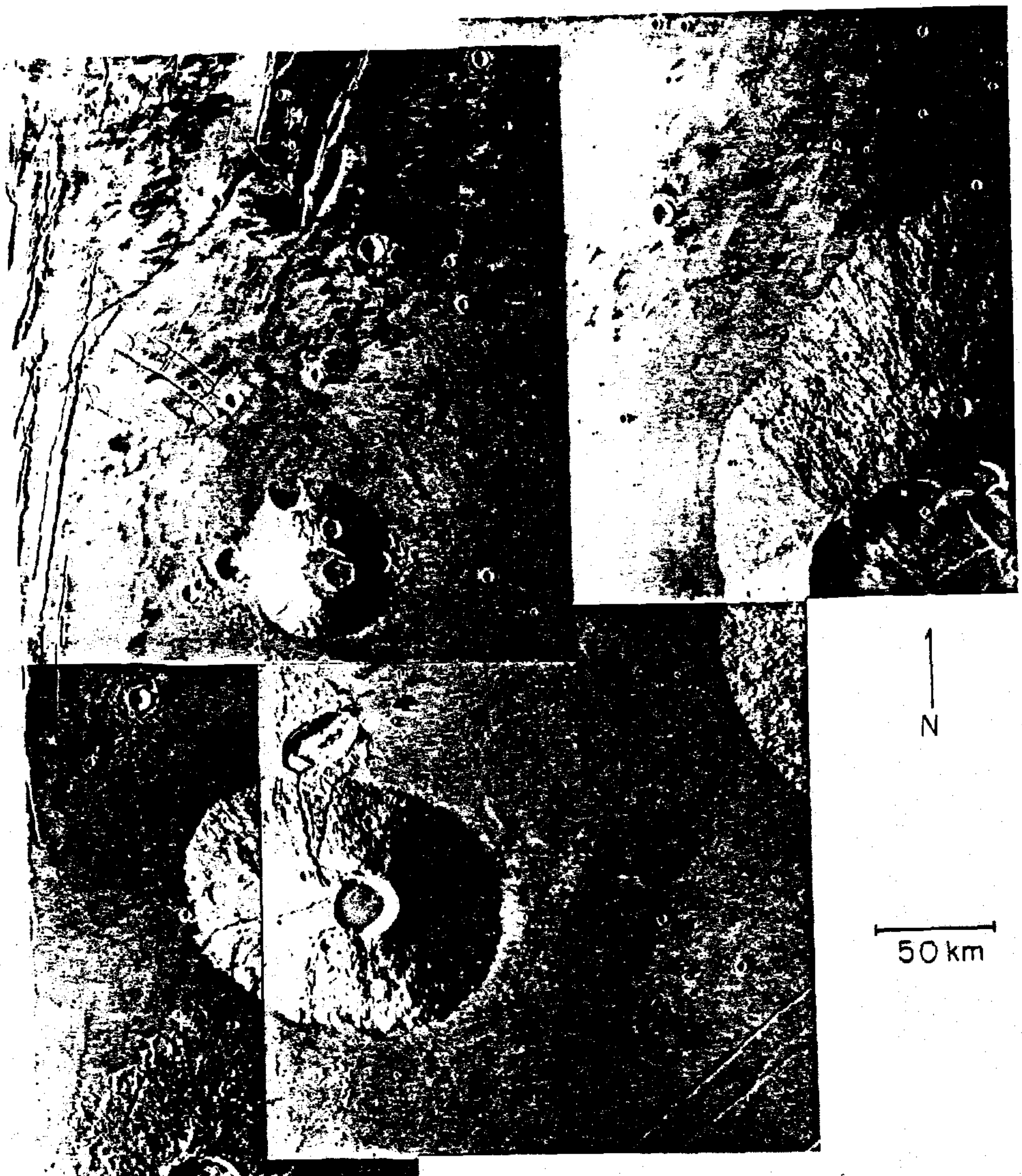
N
50 km

the subdued character of its flanks. No large channels breach the crater rim or extend down the flanks to the base of the dome. A few fine lineations and lobe-like features can be traced on the lower slopes, but their pattern is not clear due to the resolution (≈ 250 m) and illumination effects. It may be that the smooth appearance of the flanks is due to a layer of ash over older lava flows.

Uranius Tholus, about 100 km to the west of its much larger sister volcano Uranius Patera, is about 60 km in diameter and has a double crater; an 8 km-diameter crater is nested within a 15 km-diameter crater. Its height is still uncertain, but shadows indicate the summit stands 3 $\pm$ .5 km above the surrounding plains. The outer summit crater appears to have been filled to its brim to the south and west but is breached along its northern rim. Large sinuous channels issue from the caldera at these points, bifurcating and becoming narrower near the flank terminus. Numerous other fine channels extend radially down the subdued flanks from immediately below the caldera rim. These channels resemble channels eroded by explosive density currents and may have been scoured during whatever event created the inner crater. The same event probably also filled the outer crater.

The third volcano, Ceraunius Tholus (Figure 7), is ellipical, 140 km x 100 km in diameter and 10 $\pm$ 1 km in height (also determined by shadowing). Its caldera is a single, circular, 12 km crater. The northwest rim has been breached. At high resolution the hummocky surface of Ceraunius Tholus is smoothly textured by what appears to be a blanket of easily erodable fine material. Numerous <1 km-wide channels radiate from just below the crater rim. Like the slope channels on Hecates Tholus and Uranius Tholus, these channels lack levees, are non-coalescent, and exhibit discontinuous sections. Rimmed >1 km-diameter craters are also scattered on the flanks. Since most of these craters appear unrelated to the channels, they probably are not contemporaneous features.

A final intriguing feature on Ceraunius Tholus is a network of channels which head at the broken northwest rim of the caldera (Figure 8). Owing to their regular sinuousity, cross-cutting relationships, distal branching, and broken parts along the minor channels these features have been interpreted by Carr (1974) as lava channels eroded largely by the overflow of lavas from the caldera. However, the channels are extremely deep, and their hanging relationships are difficult to reconcile with the thin nature of the summit flows on steep-sloped volcanoes. Perhaps the channels were first cut by explosive volcanic density currents and later modified by lava flows. An alternative origin by water erosion has been advocated by Sharp and Malin (1975) but is not favored here because of the suggestion that the history of the volcanics of Ceraunius Tholus is similar to that of Barcena Volcano on Earth. Before addressing a detailed comparison of these two volcanoes it is noteworthy that the most prominent channel from the summit of Ceraunius Tholus empties into an impact crater and there forms a deltaic-like deposit. This curious relationship may indicate

FIGURE 8: Mariner 9B-photograph (DAS No. 089328) showing the sinuous and branching channel network from the summit caldera of Ceraunius Tholus. The most prominent channel of the network terminates in a depression interpreted as an impact crater, and there forms a deltaic-like deposit.

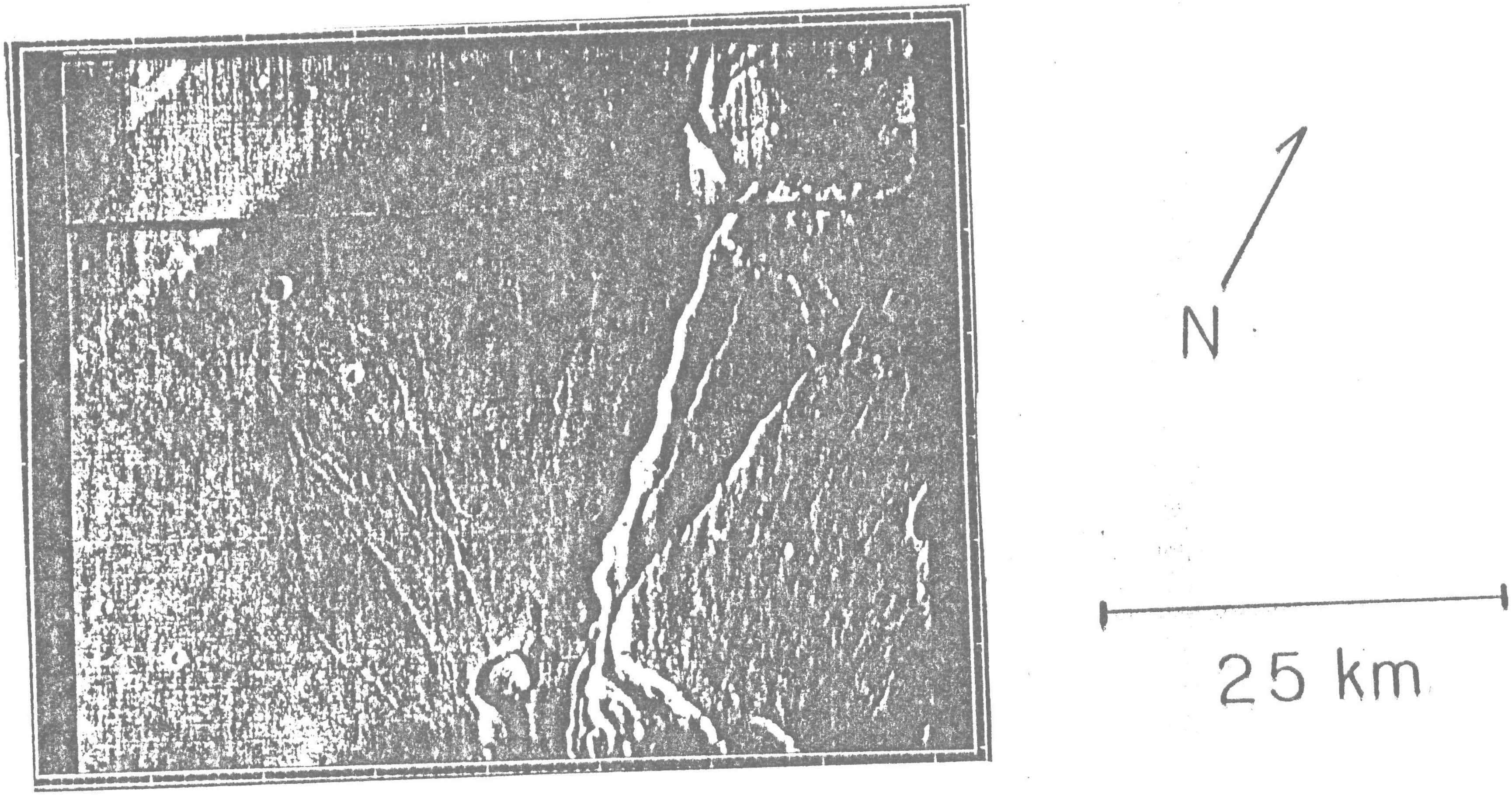
N
25 km

that one of the last eruptions of the volcano was triggered by the fall of a giant meteorite (K. Blasius, personal communication, 1977). If this interpretation is valid, it would imply the volcano has been active at least once since the flooding of the encircling plains which must be older than the meteorite crater.

Comparison of Ceraunius Tholus and Barcena Volcano. The possibility that the history of Ceraunius Tholus on Mars may be reconstructed by comparison with Barcena Volcano on Earth is suggested by the comparable morphological features of the two volcanoes. The most conspicuous features of similarity are the slope channels which radiate from below the calderas. In both cases, these channels: (1) are best developed below the rim to the first abrupt change in slope, (2) show a nearly parallel, dispersive arrangement, (3) lack levees, (4) terminate in an area of local deposition, and (5) have relatively low width/depth ratios for most of their course. Several diverse modes of origin have been proposed for the martian volcanic slope channels including: (1) water erosion nourished by seepage (Sharp and Malin, 1975), (2) lava erosion or surface collapse of lava tubes (Carr, 1973, 1974; Greeley, 1973; Carr et al., 1977), (3) tectonic fracturing and collapse of the volcanic flanks, accompanied by lava flow modification (Malin, 1977), and (4) erosion by explosive volcanic density currents.

Aqueous erosion initiated by seepage is a common mechanism of channel formation on Earth but has implications which are difficult to reconcile with the depths and radial arrangements of the slope channels on the martian cones. That is, if liquid water percolated to the surface of a martian volcano, it is doubtful that any discrete source could supply enough water to erode a large channel without first merging with water from other seepage points to produce a tributary system. Seepage may be an important modifying agent, however, forming fine convergent channels which empty into larger pre-existing channels. As discussed earlier, this relationship is apparent in the high resolution Viking photographs of Hecates Tholus.

Lava erosion, lava tube collapse and tectonic fracturing are probably viable processes on Mars, but the radial, non-coalescent, parallel pattern of the Ceraunius Tholus channels again appears to preclude these modes of origin. In addition, constructional lava channels and tubes would be expected to be penecontemporaneous with the surrounding terrain; erosional lava channels should appear relatively uniform in cross-section, being much wider than they are deep. The slope channels on Ceraunius Tholus transect smaller features on the surface of the volcano, lack levees, and show abrupt changes in both width and depth.

Creation of the Ceraunius Tholus slope channels under circumstances similar to the events which scuptured the furrows on Barcena Volcano has fewer problems. It is proposed that the martian channels developed during copious eruptions of magma and steam which spread over the slopes of the volcano as pyroclastic falls and base surge density flows. The Ceraunius channels are more widely spaced and irregular than the Barcena channels, but this probably reflects the influence of pre-eruption topography. (Ceraunius Tholus is most likely a composite volcano, whereas Barcena Volcano is a more evenly blanketed tuff cone.) The major difference between the two sets of channels is the martian features are one to two orders of magnitude larger (compare Figures 4 and 5). This same scaling problem has been discussed earlier in regard to the interpretation of lunar sinuous rilles, patterned ground, and martian volcanic constructs. Greeley (1973) suggests a possible explanation may arise from differences in gravity, effusion rate and volume. Plinian eruptions inherently are sudden events, and they erupt extremely large volumes of tephra and steam in columns which coalesce to form density flows below the caldera rim. Thus, this mechanism appears reconcilable with the dimensions of the martian channels and their development beneath the caldera rim, at least more so than erosion by water or lava.

Other features of similarity on Ceraunius Tholus and Barcena Volcano are their well-defined, circular, summit calderas, and steep slopes. The most significant distinction between the two that can be made on the basis of surface morphology is the occurrence of a diverging channel network which issues from the summit caldera, on Ceraunius Tholus, but not on Barcena Volcano. If this network and the deltaic deposit at the mouth of its principal channel are the result of lava outflow from the caldera, it may be that their creation was under circumstances similar to the formation of Delta Lavico on Barcena. Delta

Lavico was formed by a lava flow through the base of Barcena after a period of explosive activity within the dome. The lava flow caused the caldera rim to fracture above the delta. A similar sequence of events could have broken the northwest rim of the caldera on Ceraunius Tholus. Subsequent activity from the central vent would consequently direct lava down the northwest flank where it could form or follow channels and build a lava delta.

DISCUSSION AND SPECULATIONS

This paper presents evidence that some martian volcanoes, especially Ceraunius Tholus, Uranius Tholus, Uranius Patera and Hecates Tholus, show morphological features similar to terrestrial features produced by explosive volcanic density currents. Although other plausible explanations are possible for many of the individual features described, the hypothesis that hydromagmatic explosive eruptions generated by contact of rising magma with ground ice appears most compatible with what is known of martian environmental and tectonic conditions. The following discussion will focus on the origin of hydromagmatic volcanism on Mars and the implications of surface features for past environmental conditions.

Explosive Volcanism on a Planet without Moving Plates. The concept of plate tectonics where large rigid lithospheric plates move laterally over a less rigid asthenosphere is generally accepted to represent a relatively recent stage in Earth evolution which is unique among terrestrial planets (Carr, 1973; Head et al., 1977). For the planet Mars, the conclusion that the crust is stationary is reached through two observations. First, preservation of large areas of cratered terrain suggests that the martian crust has not undergone systematic destruction at plate boundaries. Second, no apparent equivalents to terrestrial spreading ridges, transform faults, fold mountains or subduction zones exist on Mars. Instead, the most noticeable martian morphological features appear to resemble terrestrial intra-plate volcanic features, such as shield volcanoes and flood basalts which typically display low indices of explosivity (Macdonald, 1972).

While the above knowledge of the tectonic evolution of Mars provides a useful framework for geologic inspection of martian volcanic features, it should not be interpreted to mean Mars is a planet devoid of pyroclastic activity. Ceraunius Tholus, Uranius Tholus, Uranius Patera and Hecates Tholus are volcanoes that do not conform with the general geomorphology and apparent structure of terrestrial shield volcanoes or flood basalts. Instead, they exhibit slope angles, caldera morphologies, and flank surfaces suggestive of explosive volcanism. This apparent variety in volcanic morphology can best be explained without calling upon magma compositions other than basalt, if a significant number of phreatic explosions generating base surges have contributed to the construction of these domes.

Although it is not usually recognized, hydromagmatic explosions are common events associated with terrestrial shield volcanoes. Since most terrestrial shields are oceanic, however, the great weight of overlying water tends to prevent gas expansion and explosion until the volcano has built close to sea level (Macdonald, 1972). On Mars where there is no ocean, base surges could occur throughout the entire constructional history of a basaltic volcano provided rising magma came in contact with a source of water. This observation implies that a fundamental factor controlling the style of martian volcanism may be the accumulation and replenishment of ground ice in the vicinity of a volcanic vent: a thick growing layer of ground ice would be conducive to explosive phenomena, whereas in areas without ground ice lavas of low viscosity would simply flow quietly.

Some erosional forms and surface textures on the martian domes described above may have alternatively been created by nuées ardentes or lava flows. Basaltic nuées ardentes, though relatively rare, have been documented on Earth from Manam Volcano, New Guinea and Ulawum Volcano, New Britain (Taylor, 1960; Melson et al., 1970), and appear to be caused by a rapid rate of magma ascension. Likewise, melting and incorporation of crustal materials above a stationary plume may explain evidence for magmatic evolution in some martian localities (Malin, 1977).

Thus, the concept that explosive volcanic processes do not necessarily demand a planet with moving plates has considerable evidence from Mars.

Environmental Constraints on Martian Explosive Volcanism. The current mean atmospheric pressure of 6 mb, mean planetary temperature of about -80°C, and low water vapor content of the atmosphere are unfavorable conditions for the persistence of liquid water on the martian atmosphere was dense, but that as this atmosphere cooled, water condensed and percolated through porous surface materials to form a thick layer of ground ice. It also suggests that the martian atmosphere has been stable and unfavorable for the recycling of ground water back to volcanic centers for an extended period of martian geologic time (probably at least the last 200 million years if the crater counts are accurate indicators of surface ages). During these recent times hydromagmatic explosions might have occurred if new vents opened in an area of extensive permafrost, but the length of the explosive phase would be limited to the depletion time of the local ice reservoir. Large volcanic constructs, such as Olympus Mons, would not be expected to show explosion related surface features but may be underlain by layers of ash flow tuffs. On the other hand, prior to 200 m.y., atmospheric conditions seem to have been more favorable for a continuous cycling of volatiles (principally CO_2, and H_2O) between the atmosphere and subsurface environment. That is, periodic changes in solar insolation due to reasons suggested by either Sagan et al. (1973) or Ward et al. (1974) may have resulted in the formation of polar layered deposits and ground ice. Replenished subsurface supplies in turn would increase the frequency of phreatic eruptions and geothermal seepage around martian volcanic centers, and thus recycle the volatiles back to the atmosphere while building steep sided domes. Reasons why this cycling process appears to have shut off on the order of 200 m.y. ago are only speculation, but perhaps a gradual and dynamic burial of ice at polar caps or beneath nonvolcanic terrains may be invoked.

REFERENCES

ARAMAKI, S. (1956). The 1783 activity of Asama Volcano, Parts I-II. Jap. J. Geol. Geogr., 27, 191-229, and 28, 11-32.

BAGNOLD, R.A. (1962). Auto-suspension of transported sediment; turbidity currents. Proc. R. Soc. Lond., A 265, 315-319, 1962.

BENJAMIN, T.A. (1968). Gravity currents and related phenomena. J. Fluid Mech., 31, 209-248.

BRYAN, W.B. (1966). History and mechanism of eruption of soda-rhyolite and alkali basalt, Socorro Island, Mexico, Bull. Volcanol., 29, 453-479.

BRYAN, W.B. (1967). Geology and petrology of Clarion Island, Mexico. Bull. Geol. Soc. Am., 78, 1461-1476.

CARR, M.H. (1973). Volcanism on Mars. J. Geophys. Res., 78, 4049-4062.

CARR, M.H. (1974). The role of lava erosion in the formation of lunas rilles and martian channels. Icarus, 22, 1-23.

CARR, M.H. (1975). The volcanoes on Mars. Sci. Amer., 234, 32-43.

CUTTS, J.A. AND BLASIUS, K.R. (1977). Models of lava erosion relevant to channel formation on Mars. Paper prepared for the Planetary Geology Field Conf. on the Snake River Plain, Idaho, 13 pp.

DAVIES, D.K., QUEARRY, M.W., AND BONIS, S.B. (1978) Glowing avalanches from the 1974 eruption of Volcano Fuego, Guatemala. Bull. Geol. Soc. Am., 89, 369-384.

ENDRODI, S.M. (1975) Petrology and geochemistry of Isla San Benedicto, Mexico, M.S. Thesis, Univ. of Oregon Dept. of Geology, 61 p.

FISHER, R.V. (1977) Erosion by volcanic base-surge density currents: U-shaped channels. Bull. Geol. Soc. Am., 88, 1287-1297.

FISHER, R.V., AND WATERS, A.C. (1969) Bed forms in base surge deposits: Lunar implications. Science, 165, 1349-1352.

FISHER, R.V. AND WATERS, A.C. (1970) Base surge bed forms in maar volcanoes. Amer. J. of Sci., 268, 157-180.

GREELEY, R. (1971) Geology and morphology of selected lava tubes in the vicinity of Bend, Oregon. Oregon Dep. Geol. Mineral Ind. Bull., 71.

GREELEY, R. (1973) Mariner 9 photographs of small volcanic structures on Mars. Geology, 1, 175-180.

GREELEY, R. AND HYDE, J.H. (1972) Lava tubes in Cave Basalt, Mount St. Helens, Washington. Geol. Soc. Amer. Bull., 83, 2397-2418.

HEAD, J.A., WOOD, C.A., AND MUTCH, T.A. (1977) Geologic evolution of the terrestrial planets. Amer. Scientist, 65, 21-29.

HEIKEN, G.H. (1971) Tuff rings: examples from the Fort Rock - Christmas Lake Valley Basin, South-Central Oregon. J. Geophy. Res., 76, 5615-5626.

HENDERSON, F.M. (1966) Open Channel Flow. Macmillan Co., New York.

LACROIX, A. (1904) La montagne Pelee et ses eruptions, Paris. Masson et Cie.

KING, J.S. AND RIEHLE, J.R. (1974) A proposed origin of the Olympus Mons escarpment. Icarus, 23, 200-317.

MACDONALD, G.A. (1967) Forms and structures of extrusive basaltic rocks. In Basalts: The Poldervaart Treatise on Rocks of Basaltic Composition, I. (H.H. Hess and A. Poldervaart, Eds.), 482 pp. Interscience Publ.

MACDONALD, G.A. (1972) Volcanoes. Prentice-Hall Inc., Englewood Cliffs, New Jersey.

MALIN, M.C. (1977) Comparison of volcanic features of Elysium (Mars) and Tibesti (Earth). Bull. Geol. Soc. Am., 88, 908-919.

MASURSKY, H., BOYCE, J.M., DIAL, A.L., SCHABER, G.G. AND STROBELL, M.E. (1977) Classification and time of formation of martian channels based on Viking data. J. Geophy. Res., 82, 4016-4038.

MATTERSON, P.H. AND ALVAREZ, W. (1973) Base surge deposits in Pleistocene volcanic ash near Rome. Bull. Volcanol., 37, 553-572.

MELSON, W.G., JAROSEWICH, E., SWITZER, G. AND THOMPSON, G. (1970) Basaltic nuées ardentes of the 1970 eruption of Ulawun Volcano, New Britain. Smithsonian Contr. to the Earth Sciences, 9, 15-32.

MOORE, J.G. (1967) Base surge in recent volcanic eruptions. Bull. Volcanol., 30, 337-363.

MOORE, J.G., NAKAMURA, K., AND ALCAREZ, A. (1966) The 1965 eruption of Taal Volcano. Science, 151, 955-960.

MOORE, J.G. AND MELSON, W.G. (1969). Nuées Ardentes of the 1968 eruption of Mayon Volcano, Philippines. Bull. Volcanol., 33, 600-620.

MUTCH, T.A., ARVIDSON, R.E., HEAD, J.W., JONES, K.L., AND SANDERS, R.S. (1976) The Geology of Mars. Princeton Univ. Press, Princeton, N.J.

OLLIER, C.D. AND BROWN, M.J.F. (1971) Erosion of a young volcano in New Guinea. Zeitschr. Geomorphologie, 15, 12-28.

RICHARDS, A.F. (1959) Geology of the Islas Revillagigedo, Mexico, 1. Birth and Development of Volcan Barcena, Isla San Benedicto (1), Bull. Volcanol., 22, 73-123.

RICHARDS, A.F. (1966) Geology of Islas Revillagigedo, Mexico 2. Geology and petrology of Isla San Benedict. California Acad. Sci. Proc., 38, 361-414.

SAGAN, C., TOON, O.B., AND GIERASH, P.J. (1973) Climatic change on Mars. Science, 181, 1045-1049.

SCHMINCKE, H.U., FISHER, R.V., AND WATERS, A.C. (1973) Antidune and chute and pool structures in the base surge deposits of the Laacher See area, Germany. Sedimentology, 20, 553-574.

SMITH, R.L. (1960). Ash flows. Bull. Geol. Soc. Am., 71, 795-842.

SODERBLOM, A., CONDIT, C.D., WEST, R.A., HERMAN, B.M., AND KREIDLER, T.J. (1974) Martian planet-wide crater distribution: Implications for geologic history and surface processes. Icarus, 22, 239-263.

TAYLOR, G.A. (1960) An experiment in volcanic prediction. Australian Bureau of Mineral Resources, Geology and Geophysics Record, 74.

THORARINSSON, S. (1967) Hekla and Katla. The share of acid and intermediate lava and tephra in the volcanic products through the geological history of Iceland. In: Iceland and Mid-Ocean Ridges. S. Bjornsson (ed.). Geoscience Soc. Iceland, 190-199.

VERHOOGEN, J. (1951) Mechanics of ash formation. Amer. J. Sci., 249, 729-739.

WARD, W.R., MURRAY, B.C. AND MALIN, M.C. (1974) Climatic variations on Mars 2. Evolution of carbon dioxide atmosphere and polar caps. J. Geophys. Res., 79, 3387-3395.

WATERS, A.C. AND FISHER, R.V. (1971) Base surges and their deposits: Capelinhos and Taal Volcanoes. J. Geophys. Res., 76, 5596-5614.

WEST, M. (1974) Martian volcanism: additional observations and evidence for pyroclastic activity. Icarus, 21, 1-11.

PART III

MODELS FOR NUÉE ARDENTE FLOW ON EARTH AND MARS

MODELS FOR NUÉE ARDENTE FLOW ON EARTH AND MARS

by

Clare E. Reimers

and

Paul D. Komar

School of Oceanography
Oregon State University
Corvallis, Oregon 97331

ABSTRACT

Equations developed to describe turbidity currents and grain flows are applied to nuée ardente flows, assuming a constant flux of tephra. The results demonstrate that a nuée ardente begins as a single layer, highly mobile, autosuspended flow that has a volume concentration of solids less than 9% (Bagnold's "collision limit" for a dispersion of cohesionless grains). The flow velocity decreases, however, as the nuée ardente moves downslope under the influence of gravity and drag forces. As a result, the flow develops into a two-layer system consisting of a high concentration (9-55%), pseudo-laminar underflow and an overriding turbulent cloud. Debris in the underflow is supported largely by a grain-dispersive pressure until on slopes too low to drive the flow, it rather suddenly stops, freezing in position. This change in flow behavior is offered as an explanation for the observed

occurrence of proximal erosional channels and distal massive deposits along the courses of most nuées ardentes.

The relationships for flow velocity and driving force terms are applied to hypothetical nuées ardentes and base surges on the planet Mars. The solutions indicate that if an eruption column large enough to coalesce into an explosive volcanic density current was generated on Mars, the velocities and driving forces of the current would be comparable to values for terrestrial flows, but the martian flow would probably travel farther and disperse debris over greater distances.

INTRODUCTION

When a dispersion of solid grains moves downslope under the pull of gravity, the physical properties of the flow (that is, its velocity, density and thickness) can be determined quantitatively if the mechanisms that support grains above the bed are known. This approach has been employed by Komar (1971), 1977, 1978) to predict the flow parameters of marine and subaerial turbidity currents (grain support is by fluid turbulence), by Lowe (1976) to evaluate the properties of subaqueous and subaerial grain flows (grain support is by grain interactions providing a dispersive pressure), and by Hampton (1975) to study the competence of fine-grained debris flows (grain support is by matrix strength).

In this paper, a similar treatment is given to nuées ardentes, a highly mobile and destructive species of gravity current produced by volcanic blasts (Figure 1). As attested by observational accounts, nuées ardentes emerge onto the slopes of volcanoes as hot, highly turbulent, one layer, low concentration dispersions of ash and magmatic gases (Lacroix, 1903; Anderson and Flett, 1903; Moore and Melson; 1969; Davies et al., 1978). Initial momentum is imparted to the flow by explosion and column collapse, and their velocities may excede 50 m/sec. Once in motion, however, the passage of a nuée ardente becomes controlled by a balance of gravity and drag forces, and it develops into a flow with two parts: (1) a high concentration, incandescent, pseudolaminar underflow, or avalanche, and (2) an overriding, turbulent, gas and dust cloud. Both portions travel laterally, but the lighter cloud is less influenced by topographic obstructions, and hence, may become separated from its underlying avalanche.

In order to explain how the physical properties of a nuée ardente change along its course and the influence of these changes on the formation of ignimbrites, the present paper summarizes the basic equations developed by Bagnold (1962), Middleton (1967), Benjamin (1968) and Komar (1971, 1977) for turbidity currents, and those developed by Bagnold (1954, 1956) and Lowe (1976) for grain flows. These equations are then utilized in a constant particle flux model to evaluate the flow densities, thicknesses, and bottom stresses required to erode and transport debris at reported speeds and slopes for two nuée ardente flows. Inasmuch as we first became interested in the problem of the physical properties of nuées ardentes while studying evidence for their

FIGURE 1: A nuée ardente. This particular photograph shows the May 2, 1968 eruption of Mayon Volcano, Philippines. The front of the avalanche portion of the nuée ardente is visible in the lower center. The remainder of the avalanche is obscured by the trailing cloud of gas and dust. The picture is taken from Moore and Melson (1969).

occurrence on Mars (Part II), the flow mechanics of a nuée ardente in a martian environment are also discussed and probable flow parameters are evaluated.

BASIC THEORY DISTINGUISHING TURBIDITY CURRENTS AND GRAIN FLOWS

Criteria to distinguish turbidity currents from grain flows have been based largely on the theoretical and experimental work of Bagnold (1954, 1956, 1962) regarding dispersions of cohesionless grains. He found that in order for a density current to remain fully turbulent (Reynolds number > 3000) frictional effects of random contacts between grains must be negligable. An upper "collision limit" to the possible range of concentrations for a fully developed turbidity current is thus suggested. Bagnold (1962) reasoned this limit to occur at a grain concentration where the free distance between grains is equal to the grain diameter (for sand sized grains this occurs at a volume concentration of about 9%). Increases in concentration above the collision limit tend to increase the overall resistance to flow and dampen out turbulence. Hence, the flow rapidly develops into a pseudo-laminar grain flow.

In addition to the above criterion being satisfied, the flow of a turbidity current must maintain a sufficient gravitational energy to sustain the turbulence necessary to keep sediment in suspension (and to overcome the frictional resistance at the bottom and upper interface of the flow). Bagnold (1962) called this condition "autosuspension". Balancing the power provided to the flow by the downslope component of gravity acting on the suspended grains against the power expended in lifting the sediments at the same rate they are falling relative to the fluid (their fall velocity, w), and the power lost due to the bottom and surface drag, Bagnold obtained the relation

$$(\rho_2 - \rho_1)gNh(\bar{u}\sin\beta - w) = (\tau_0 + \tau_i)\bar{u} \tag{1}$$

in which ρ_2 is the flow density, ρ_1 is the density of the surrounding fluid, g is the acceleration of gravity, N is the volume concentration of solids, $\bar{u}$ is the average flow velocity, h is the flow thickness, $\sin\beta$ is the slope, τ_0 is the bottom drag, and τ_i is the drag on the upper interface of the flow. N is assumed constant throughout the flow thickness and is related to the flow density by

$$N = \frac{\rho_2 - \rho_1}{\rho_s - \rho_1} \tag{2}$$

where ρ_s is the density of the solid grains. Equation (1) necessitates an "autosuspension limit" in which

$$\bar{u} \geqq w/\sin\beta\ . \tag{3}$$

Otherwise, the available power of the flow is insufficient to maintain sediment in autosuspension, and the flow collapses into a high concentration grain flow.

EQUATIONS OF MOTION GOVERNING TURBIDITY CURRENTS AND GRAIN FLOWS

Laboratory models of channelized turbidity currents show that as an individual flow moves away from its source it quickly entrains fluid to form a flow consisting of four main parts: a head, a neck, a body, and a tail (Figure 2; Kuenen, 1950; Keulegan, 1957, 1958; Middleton, 1966-1967). The head of a turbidity current has a characteristic shape and flow pattern which sweeps fluid and sediment forward and upward. The velocity of the head can be predicted from a balance of the hydrostatic pressure force against the resisting horizontal momentum of the overlying fluid (Benjamin, 1968) which yields the simple formula

$$v = C \left[\frac{\rho_2 - \rho_1 \; gh}{\rho_1}\right]^{1/2} \qquad (4)$$

where v is the velocity, and C is a dimensionless coefficient which Keulegan (1957, 1958) and Middleton (1966) showed equal to approximately 0.75 for turbulent flow. It should be noted that equation (4) does not depend on the bottom slope because the head is being driven by the piezometric pressure difference between it and the surrounding fluid, not by gravity (Benjamin, 1968).

The motion of the body is described by a Chezy-type equation derived by balancing the gravity force against the retarding-frictional drag for uniform flow (Middleton, 1966; Komar, 1971), and is expressed in the form

$$u = \left[\frac{\rho_2 - \rho_1}{\rho_2} \, gh \, \frac{\sin \beta}{(1 + \alpha) \; c_f}\right]^{1/2} \qquad (5)$$

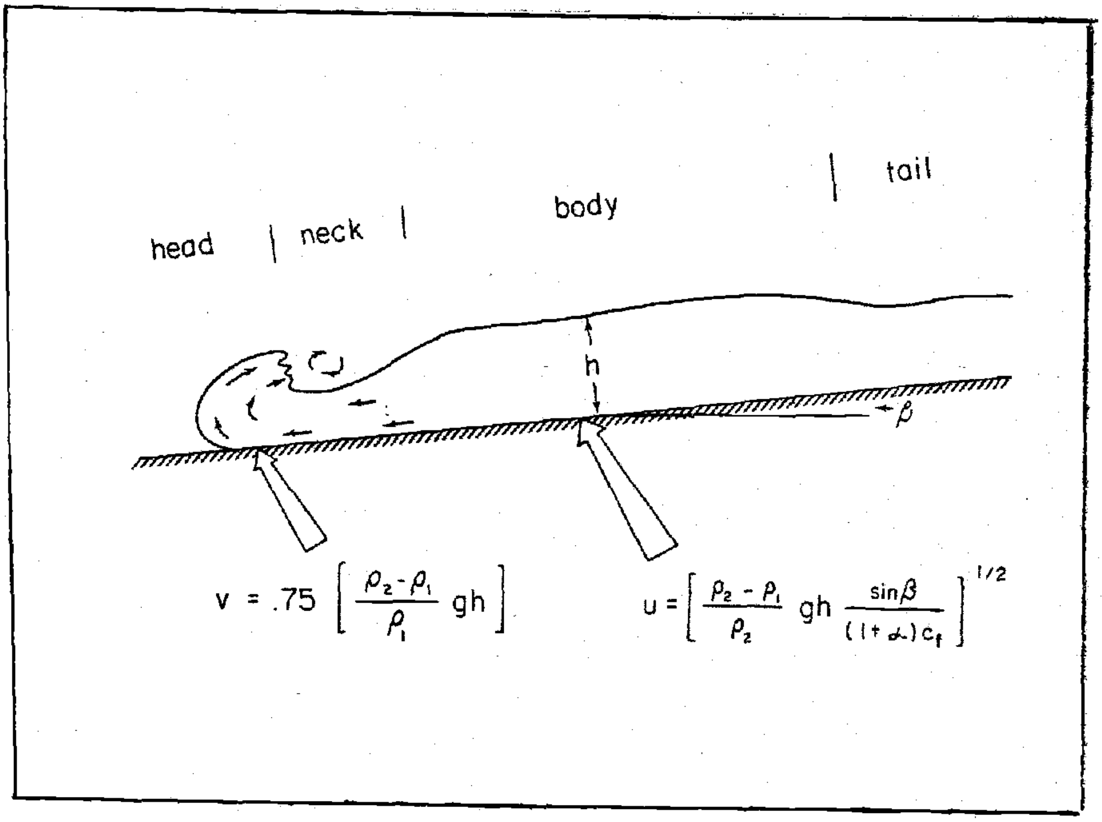

FIGURE 2: The divisions and governing equations of a turbidity current

where c_f is a drag coefficient, and α is the ratio of the drag on the flow at the upper surface to the drag on the bottom. As indicated, equation (5) applies to nonaccelerating uniform flow, that is, when the velocity, density, and thickness are constant in the direction of the flow. Komar (1977) demonstrates how this equation is in effect the momentum flux equation for steady uniform flow. Using equations (5-7) of that paper, an expression for the total drag of the flow becomes

$$\tau_0 + \tau_i = (\rho_2 - \rho_1)ghs\sin\beta \ . \qquad (6)$$

When the flow is nonaccelerating, the driving force equals the opposing drag, and so equation (6) represents the erosive power of a steady uniform flow.

According to equation (5) for the flow velocity of a turbidity current, if the bottom slope $\sin\beta$ decreases in the direction of flow, the velocity $\bar{u}$ will also tend to decrease. A point will be reached where $\sin\beta$ and $\bar{u}$ are sufficiently low that the predominance of material in the flow will have settling velocities greater than the "autosuspension" settling velocity according to equation (3). At that point the flow will deflate, expressed in channelized flows as an increase in the concentration of grains in the flow. If the concentration should rise above about 9%, then grain to grain stresses become more important than fluid stresses, and the flow velocity $\bar{u}$ can no longer be defined by equation (5). Instead, the grain stresses can be resolved into components normal, P, and tangential, T, to the bottom which are related by

$$T = P\tan\alpha \tag{7}$$

where α is an angle of internal friction. Bagnold (1954) showed empirically that where grain collisions dominate, flow is inertial, and both stresses, T and P, can be related to the rate of shearing and concentration of the flow. This relationship gives

$$T = a_o \rho_s \Lambda^2 D^2 (du/dy)^2 \tag{8}$$

in which a_o is a constant proportional to sin α, D is the mean particle diameter, du/dy is the velocity gradient of the sheared suspension, and Λ is the linear grain concentration which is a dimensionless measure of grain concentration related to the volume concentration N by

$$\Lambda = \frac{1}{(N_o/N)^{1/3} - 1} \quad . \tag{9}$$

N_o is the closest packing volume concentration and is dependent on the shape and size distribution of the suspended grains. For most natural, well-sorted sediments, N_o is approximately equal to 0.65 (Bagnold, 1956).

Steady and uniform grain flow exists only on a slope where tan α= tan β. Bagnold's (1954) empirical determinations imply that tan α should be between 0.32 and 0.40, if the flow is in the inertial regime. More recently, however, he has suggested that his experimental dispersions involving paraffin and lead stearate spheres did not adequately represent natural systems, and that tanα should be equated with the angle of repose, that is, tan α = 0.63.

Equating equations (6) and (8) for the tangential grain shear at any select point y above the bed of a steady uniform flow yields

$$(\rho_2 - \rho_1)g(h - y)\sin\beta = a_o\rho_s(\Lambda D)^2(du/dy)^2 \quad . \tag{10}$$

Solving equation (10) for du/dy and integrating with the condition that at y = 0, u = 0, yields for inertial flow

$$u = \frac{2}{3}\left[\frac{(\rho_2 - \rho_1)g\sin\beta}{a_o\rho_s}\right]^{1/2} \frac{1}{\Lambda D}\left[h^{3/2} - (h - y)^{3/2}\right]. \tag{11}$$

This solution is essentially the same as the velocity equation for tangential grain flow determined by Lowe (1976, equation 13b).

To solve for the average flow velocity $\bar{u}$, equation (11) may be integrated over the entire flow thickness h to yield

$$\bar{u} = \frac{2}{5}\left[\frac{\rho_2 - \rho_1}{a_o\rho_s}\; g\sin\beta\right]^{1/2} \frac{1}{\Lambda D}\; h^{3/2} \;. \tag{12}$$

A comparison of equations (5) and (12) illustrates that once interactions between sheared grains become sufficiently intense to produce a grain flow, the resulting flow velocity is no longer primarily a function of the flow thickness and downslope component of gravity, but is highly dependent on grain size and concentration as well.

In the development of models for the flow of natural turbidity currents or grain dispersions (such as will be presented throughout the remainder of this study), the situation is somewhat complex because the flow is neither continuously steady or uniform. The total volume of the mixture, however, is conserved and a separate continuity equation may be written for each material (Komar, 1971, 1977).

Considering only the grains within the flow, the total particle flux per unit width becomes

$$\text{particle flux} = F = Nh\bar{u} \quad . \tag{13}$$

If one considers successive cross sections of the flow as it moves along its path

$$N_{n+1}h_{n+1}\bar{u}_{n+1} = N_n h_n \bar{u}_n + q_s \ell \tag{14}$$

where the subscript n may range from 1 to ∞, and ℓ is the distance separating the two points of measurement. When negative in value, q_s is the average rate of particles lost per unit area due to deposition; when positive, q_s is the average rate that particles are gained by erosion along the flow path, ℓ.

It should be noted that equation (14) is strictly valid only if the modelled flow does not spread laterally, and if the sediment concentration of flow density is constant vertically through its thickness (Komar, 1977). The later assumption is reasonably valid if the flow is autosupended or if the particle concentration is sufficiently high to create a non-shearing, pseudo-plastic sediment plug or debris flow (Lowe, 1976). For models of intermediate concentration grain flows, however, errors will result from the assumption of a constant vertical concentration, but these should not significantly alter the results.

PHYSICAL PROPERTIES AND FLOW MECHANICS OF NUÉES ARDENTES

Development of a Constant Particle Flux Model

Documentation of the turbulent, highly mobile nature of nuées ardentes poses problems for explaining the fact that most nuée ardente deposits have many characteristics common to more sluggish, high concentration flow deposits such as mud-flows and fluxoturbidites (Sparks, 1976). One approach is to consider the physical properties of a nuée ardente avalanche and how these properties are affected as the flow changes speed along a varying slope. Timed photographic sequences of individual eruptions provide documentation of flow speeds and directions (Table I). Unfortunately, no direct measurements of flow densities and thicknesses exist owing to the hazard involved and the fact that the overriding gas and dust clouds tend to obscure any view of the glowing avalanche portion of the nuée ardente. Indirect estimates of thicknesses of just the avalanches have been deduced from the scraping of bark from trees or the scouring on valley walls along the flow path (Davies et al., 1978; Macdonald and Alcaraz, 1956). These data indicate typical heights of a few meters to 10's of meters, but because the presence of an obstacle in the path of a moving avalanche would cause fragments to be thrown vertically, Davies et al. (1978) caution that these estimates are probably too high. To deal with this problem

TABLE I Physical properties for the avalanche portion of the St. Augustine and Mayon Nuées Ardentes obtained from timed photography and a constant particle flux model. $\rho_s = 2.0 g/cm^3$, $c_f = .01$. Photography data is from Stith et al. (1977) and Moore and Melson (1969).

Elevation of the front (m)	Cumulative slope distance (m)	Approximate slope (sinβ)	Velocity (m/sec)	Flow density (g/cm^3)	Sediment volume concentration	Thickness (cm)	Driving force ($dynes/cm^2$)
ST. AUGUSTINE VOLCANO:							
1200- 240	0-3040	.316	50	.067	.034	807	1.65×10^4
240- 120	3040-3890	.141	21	.408	.204	320	1.80×10^4
120- 100	3890-4170	.071	13	.600	.300	352	1.47×10^4
100- 70	4170-4470	.100	13	.642	.321	329	2.05×10^4
70- 50	4470-5030	.036	6	.982	.491	466	1.61×10^4
50- 0	5030-6480	.035	6	.980	.490	467	1.57×10^4
MAYON VOLCANO:							
1360-1260	0- 200	.500	63	.107	.053	815	4.23×10^4
1269-1150	200- 420	.500	47	.256	.128	452	5.65×10^4
1150- 980	420- 880	.370	29	.444	.222	422	6.79×10^4
980- 830	880-1230	.429	38	.328	.164	436	6.00×10^4
830- 690	1230-1650	.333	51	.204	.102	522	3.44×10^4
690- 650	1650-1810	.250	9	1.068	.534	565	1.48×10^5
650- 600	1810-2030	.227	30	.378	.189	479	4.08×10^4

continued onto next page...

TABLE I continued...

Autosuspension limiting velocity (m/sec)	Suspended pumice diameter (mm)	Suspended lithic diameter (mm)
15.8	5.4	2.3
3.0	0.9	0.4
0.9	0.3	0.1
1.3	0.4	0.2
0.2	0.1	0.05
0.2	0.1	0.05
31.5	10.1	4.8
23.5	8.5	3.5
10.7	3.5	1.5
16.3	5.6	2.4
17.0	6.0	2.5
2.3	0.7	0.3
6.8	2.2	0.9

a model which utilizes the continuity and velocity equations developed for turbidity currents and grain flows is useful. Numerical solutions for the turbulent stages of flow have been determined by Sparks et al. (1978) for hypothetical pyroclastic flows assuming column collapse and uniform radial spreading. Their model does not take into account changes in flow density and thickness, and thus their solutions become increasingly inexact away from the source. To eliminate these problems we have developed a model which considers both turbulent and non-turbulent flow conditions. Our model assumes that initially the flow is fully turbulent and driven by the hydraulic head of suspension so the thickness is related to the initial velocity by equation (4). Solving for h gives

$$h = \frac{v^2 \rho_1}{(0.75)^2 (\rho_2 - \rho_1) g} \quad . \tag{15}$$

Substituting this expression and equation (2) into equation (13), the initial particle flux per unit width becomes

$$F = \frac{v^3 \rho_1}{(\rho_s - \rho_1)(.75)^2 g} \tag{16}$$

and may be evaluated from photographic measurements of v. If the flow is loosing or gaining particles, F must change accordingly (equation 14). Fortunately for the model, glowing avalanches generally deposit little or no tephra on the steep slopes of their volcano (except coarse blocks carried as traction load). Thus, the particle flux F can be assumed to be nearly constant until the flow reaches the base of the volcano.

If F is constant, equation (5) can be solved for the variable flow density ρ_2 and by incorporation of equation (15) rewritten as

$$\rho_{2_{n+1}} = \frac{F(\rho_s - \rho_1)g\sin\beta}{(\bar{u}_{n+1})^3 c_f} \tag{17}$$

Estimates for the thickness simplify to

$$h_{n+1} = \frac{F}{N_{n+1}\ \bar{u}_{n+1}} \tag{18}$$

From these equations it is possible to estimate the density (concentration) and thickness a nuée ardente avalanche would have at successive locations downslope where the velocity and gradient are known, provided it remains turbulent. However, if the flow should decelerate and the sediment concentration rise above about 9%, grain flow theory must be applied.

Utilizing equation (12) for the velocity of a steady uniform high concentration nuée ardente avalanche where $\rho_2 >> \rho_1$, a ratio of velocities at successive points simplifies to

$$\frac{\bar{u}_n}{\bar{u}_{n+1}} = \frac{\Lambda_{n+1}}{\Lambda_n}\ \frac{N_n \sin\beta_n}{N_{n+1}\sin\beta_{n+1}}\ \frac{h_n}{h_{n+1}}\ . \tag{19}$$

If initial values of sediment concentration and thickness have been determined, this expression contains only two unknowns, h_{n+1} and N_{n+1}. Combining equation (19) with the continuity equation (14) yields an expression with only one unknown. Due to the complexity of this equation we found the best method of solution was by computer iteration.

It should be recognized that for a nuée ardente to be entirely supported by dispersive pressures requires slopes at or above the static angle of repose (about 32°). Volcano flanks are, of course, seldom that steep. This is not a serious problem, however, because several processes inherent to nuée ardentes should aide dispersive pressures in maintaining a dispersion against the force of gravity: (1) the gases interstitial to the grains may be denser than the gases in the overlying cloud creating a buoyancy effect (Tazieff, 1970; Wilson, 1976); (2) lift forces and small scale turbulence may be generated by escaping volatiles emitted from incandescent particles; (3) dispersed fines mixed with interstitial gases may act to support larger grains while promoting higher flow velocities by increasing the density difference between the flow and its surroundings; and (4) shear may be transmitted downward to the basal avalanche from the upper turbulent cloud. The possibility of such processes creating "modified grain flows" which are mobile over low slopes in a subaqueous or subaerial environment has been discussed by Middleton (1970) and Lowe (1976). It seems clear that their conclusions also apply to nuées ardentes.

Model Results

Mayon Volcano, Philippines, and St. Augustine Volcano, Alaska, are two volcanoes where flow velocities and directions of recent nuée ardente eruptions have been recorded by timed photography (Moore and Melson, 1969; Stith et al., 1977). Hence, each record provides adequate information such that an analysis of nuée ardente dynamics is possible using a constant particle flux model.

Table (I) shows calculated flow densities and thicknesses at the midpoint of each interval of the observed travel distance for the Mayon and St. Augustine volcanoes. The density of the material in suspension was assumed equal to 2.0 g/cm^3, a value intermediate between the density of pumice and most lithic fragments. α was assumed equal to zero since the resistance at the upper interface of a nuée ardente would be negligible compaed to the bottom drag. The best choice for a value for c_f was uncertain. c_f is a resistance coefficient related to Darcy's f by

$$c_f = \frac{f}{8} \quad . \tag{20}$$

f may be obtained from the well-known Moody diagram for the behavior of resistance coefficients (Kersey and Hsu, 1976). For fully turbulent flow the resistance coefficient is independent of Reynolds number and dependent only on the ratio of the flow thickness to a length parameter characteristic of the surface roughness. This ratio is called the relative roughness h/k_s, and is inversely related to c_f (Henderson, 1966; Komar, 1978).

For subaqueous turbidity currents c_f is generally taken to be on the order of .0035 to .005 (Johnson, 1964; Komar, 1969, 1971, 1977).

These values are somewhat lower than would be expected for the flow of a nuée ardente over a rough volcanic flank where the relative roughness h/k_s would be much less. Sparks et al. (1978, p. 1732) estimated c_f should vary in the range of .02 to .005. They assumed the value of k_s was 1.0 cm and utilized Schlichting's (1960, p. 521) equation for the turbulent flow of gases through an open channel. For this analysis of nuée ardente flow the value of c_f was chosen at .01. We assumed a constant value for simplification, although we realize changing flow parameters do vary c_f somewhat. The variations, however, are small in comparison to the other uncertainties in the calculations.

Figure 3 shows the progressive changes in average slope, velocity, flow density and thickness for the Mayon and St. Augustine nuées ardentes based on the constant particle flux model presented above. In general, a decrease in slope causes a decrease in the kinetic energy of the flow which decreases the turbulence, thus deflating the flow and increasing ρ_2. An increasing slope has the opposite effect.

More specifically the results in Table (I) provide estimates for nuée ardente flow densities and thicknesses, and indicate that the densities agree initially with Bagnold's (1956) criteria for turbulent autosuspended sediment gravity flow (ie, $N<.09$), while the thicknesses agree with Davies et al. (1978), and Macdonald and Alcaraz's (1956) indirect estimates of probable flow heights. At distances of kilometers from the vent, however, the model substantiates that nuée ardente avalanches probably deflate and flow in pseudo-laminar fashion as high concentration dispersions similar to grain flows.

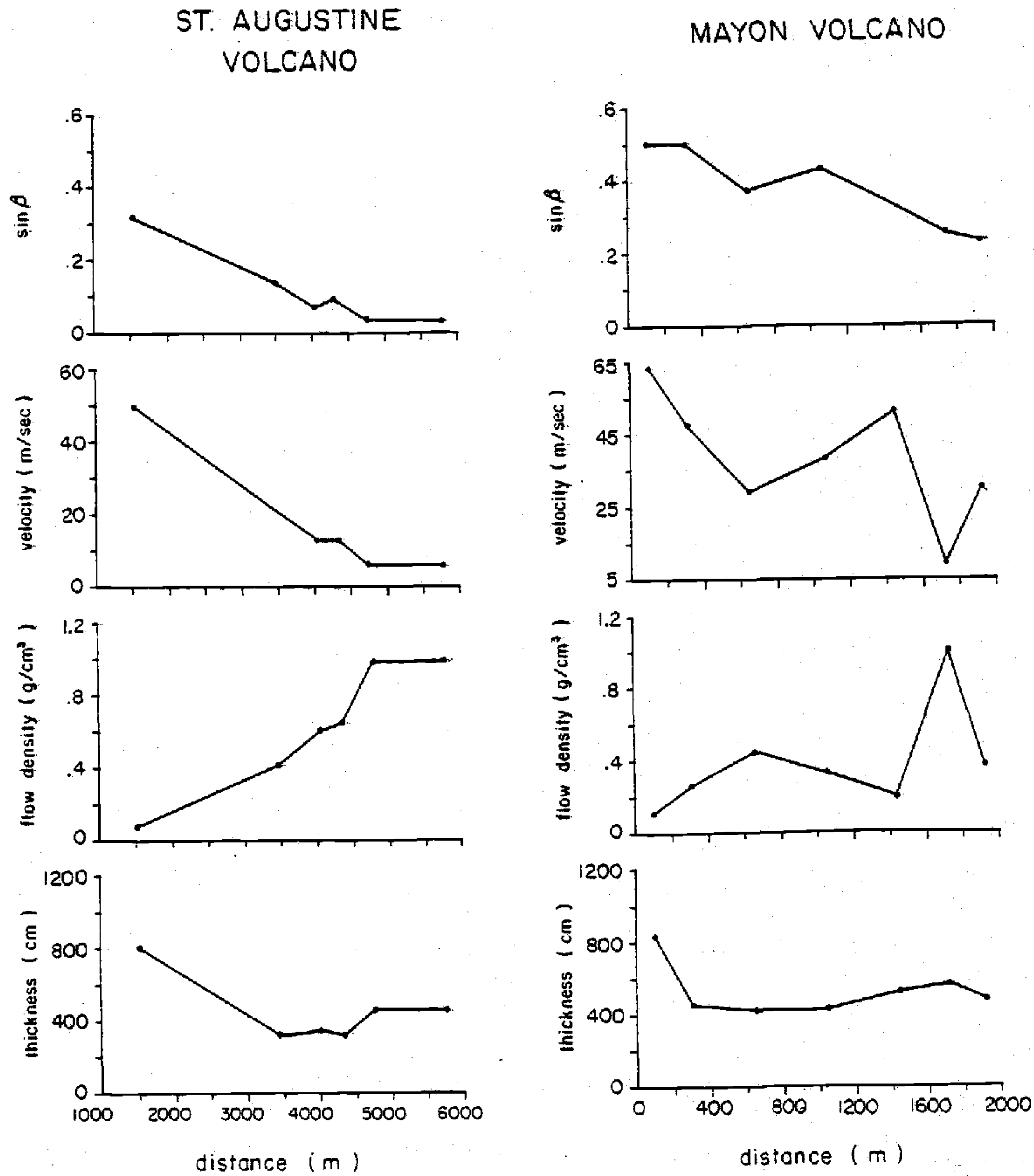

FIGURE 3: Flow parameters of nuées ardentes from the 1976 eruption of St. Augustine Volcano, Alaska and the 1968 eruption of Mayon Volcano, Philippines based on timed photography and a constant particle flux model.

Middleton (1967) and Middleton and Hampton (1976) have shown that as the lower portion of such a grain flow decelerates its driving force will diminish to less than is necessary to sustain the sediment supporting mechanism (dispersive pressure). At this point the grain flow will be emplaced by "rapid freezing" to produce a deposit that preserves the structure and texture of the flow prior to emplacement. Thus, the poor sorting and inverse grading common to the main portion of ignimbrite flow units (Sparks, 1976; Sparks et al., 1973; Sparks and Walker, 1973) is explained by the modeling conclusion that a nuée ardente avalanche must develop a high sediment concentration supported largely by dispersive pressure.

Other results contained in Table (I) include calculations of the autosuspension limits, corresponding autosuspended grain diameters and driving forces of the Mayon and St. Augustine nuées ardentes. The autosuspended grain diameters were determined according to equation (3) and Figure (4). An interesting aspect of the autosuspension limiting velocities is that only initial values correspond to the -3 to 0 Md ϕ particle sizes found in most ignimbrite sequences (Sparks, 1976; Walker, 1971). Since the ignimbrites usually occur as fan-like deposits distributed radially for several kilometers beyond the base of their source volcano, another particle support mechanism besides turbulence is necessary to explain the transport and deposition of these coarse components. This mechanism is, of course, dispersive pressure created by grain to grain interactions, and aided by the shear and lift forces discussed earlier.

FIGURE 4

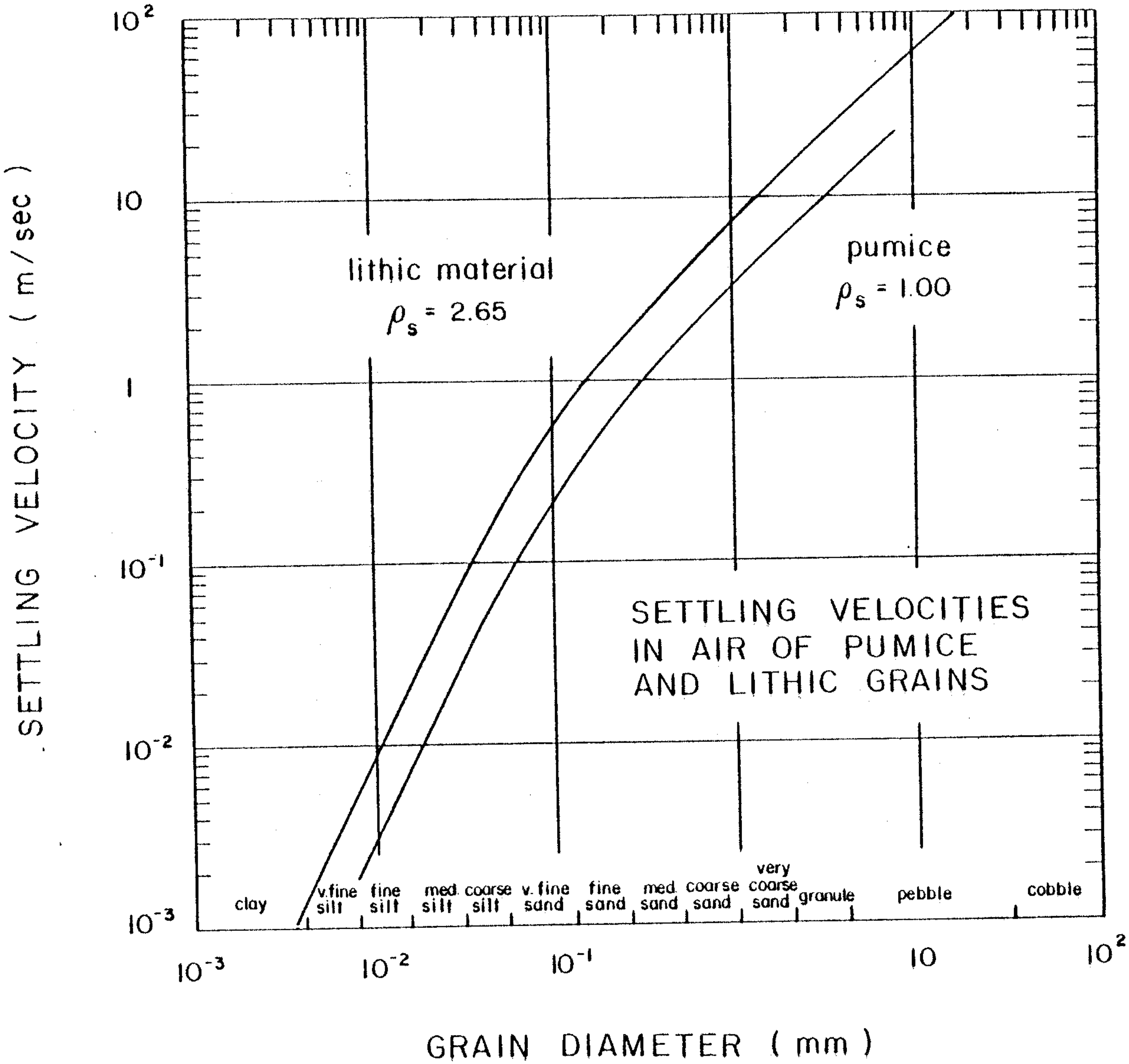

SETTLING VELOCITIES IN AIR OF PUMICE AND LITHIC GRAINS
lithic material
$\rho_s = 2.65$
pumice
$\rho_s = 1.00$
SETTLING VELOCITY (m/sec)
GRAIN DIAMETER (mm)
10^2
10
1
10^{-1}
10^{-2}
10^{-3}
10^{-3}
10^{-2}
10^{-1}
10
10^2
clay
v.fine silt
fine silt
med. silt
coarse silt
v. fine sand
fine sand
med. sand
coarse sand
very coarse sand
granule
pebble
cobble

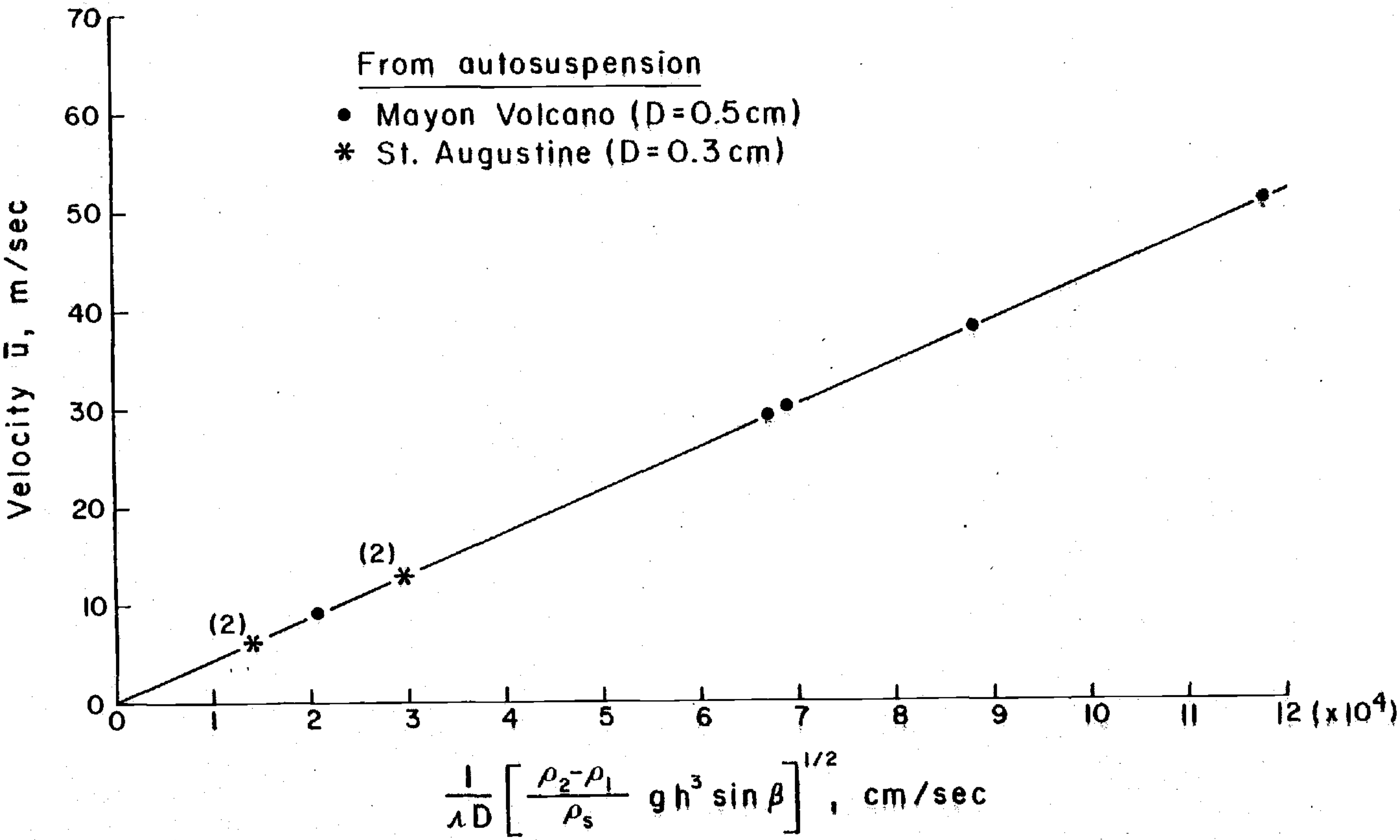

FIGURE 5: Relationship between mean flow velocity and predicted velocity in inertial high concentration nuée ardente avalanches.

The driving force terms $(\rho_2 - \rho_1)ghs\sin\beta$ for both the nuées ardentes studied are the same within an order of magnitude and sufficiently high to suggest nuées ardentes must initially be erosive agents. Komar (1978) compares the driving forces of marine turbidity currents, rivers, and the Lake Missoula flood. In comparison to Komar's results, the erosive powers of the Mayon and St. Augustine nuées ardentes are far greater than river flow erosion but correspond closely to documented events of submarine turbidity currents and catastrophic subaerial flooding. This observation leaves little doubt that nuées ardentes are capable of producing channel-like features on the flanks of composite volcanoes and domes (Part II).

Finally, plots of the velocities listed in Table I versus $1/\Lambda\ D[(\rho_2-\rho_1)/\rho_s gh^3 \sin\beta]^{1/2}$ for the nonturbulent stages of the Mayon and St. Augustine nuées ardentes (N>.09) are shown in Figure 5. The slopes of the coincident lines provide an empirical value of .044 for the combined constant terms $2/5a_0^{-1/2}$ in equation (12). Therefore, the constant a_0 alone is equal to approximately 83. These values are significant because (1) the two modeled flows yield identical values, and (2) they differ considerably from Bagnold's (1954) empirical constants determined from experiments using confined dispersions of paraffin and lead stearate spheres in water and water-glycerine-alcohol mixtures.

It is not intuitively obvious, but our modeling approach assumed a_0 does not change with concentration for any individual flow. That is, by taking a ratio of velocities at successive points and eliminating the constant terms $2/5a_o^{-1/2}$ to yield equation (19), we predetermined a linear relationship between $\bar{u}$ and $1/\Lambda D[(\rho_2-\rho_1)/\rho_s gh^3 \sin\beta]^{1/2}$ for each modeled flow. But there was nothing in our model that demanded the slope of the lines in Figure 5 should be the same for different flows. Hence, the identical values for a_o that result from the Mayon and St. Augustine models are further evidence that our model adequately predicts the physical parameters of nuées ardentes.

Whether Bagnold's (1954) experimental constants may characterize other natural systems at corresponding grain concentrations is difficult to judge. Actually, Bagnold did not use a_o in his equations, but instead he included two parameters, a constant a_i and $\sin\alpha$. In his experiments, he found $\tan\alpha$ to be nearly constant at .32 for inertial flows where Λ<12. The constant a_i he measured empirically as .042. These values yield a corresponding value of a_o equal to .013. Lowe (1976) has suggested Bagnold's experimental dispersions differed from natural flows because natural flows are not fully confined and have different elastic properties which may create greater surface resistance. Lowe also points out that $\tan\alpha$ is an empirical measure of T/P (equation 7). Since a_o is proportional to $\sin\alpha$, it too is a measure of T/P and will be large when the normal components in an inertial dispersion outweigh the tangential components (equations 7 and 8). As discussed earlier, nuées ardentes are inherently modified by gas emission, dispersed fines, internal turbulence and transmitted shear. These combined effects enhanse the normal component P, and therefore values of a_0 can be explained as a consequence of the physical properties of the system rather than an artifact of our model.

FURTHER APPLICATIONS

General Statement

The quantitative approach to the analysis of nuées ardentes by a particle flux model is applicable to the study of other types of sediment gravity flows or to nuées ardentes under different environmental conditions. The example to be considered here is the flow of an explosive volcanic density current (ie., either a nuée ardente or a similar but hydromagmatically generated base surge) on the planet Mars. Morphological features associated with certain martian volcanoes have been identified in Part II as erosional channels and depositional structures similar to features formed by terrestrial nuées ardentes and base surges. For these interpretations to be correct, it is pertinent to demonstrate that the mechanics of volcanic density currents on Mars compare with those of flows on Earth.

Flow of Explosive Volcanic Density Currents on Mars

The mean density of the martian atmosphere is only $2x10^{-5}g/cm^3$ (Seiff and Kirk, 1976, Figure 2), two orders of magnitude less than Earth's. This observation has two consequences in regards to the analysis of explosive volcanic density currents in a martian environment. First, it would appear that atmospheric entrainment could not significantly fluidize a density current on Mars. Hence, a martian nuée ardente or base surge could maintain mobility only so long as the turbulence and/or dispersive pressure on the initial gas phase are sufficiently great to support the weight of suspended particles. Secondly, martian density flows would exhibit a greater coherency than the same flows in a terrestrial atmosphere. This conclusion is reached by consideration of the processes which cause a fluidized system to expand and dissipate. Terrestrial nuée ardente avalanches expand and form a turbulent cloud portion because hot juvenile gases are lighter than the surrounding medium, rise, and promote advective mixing. However, the same juvenile gases would not be buoyant in a martian atmosphere, and gas exchange would be governed by much slower diffusion. This process could be envisioned as analogous to the dilation of a subaerial water-saturated sand flow (Lowe, 1976).

It would thus appear that a preliminary condition for the formation of a martian volcanic density current is that a great volume of volatile materials be produced at the vent area. Assuming this, the initial lateral velocity of an explosive volcanic density flow would be due to the momentum acquired during eruption and to the lateral pressure force acting on the gas-solid system (Equation 4). However, if a flow continued over a sloping ground, the velocity should then become governed by a balance between the component of gravity acting on the flow and the retarding grain shear stress (Equations 5 and 12).

Table (II) lists values for the driving force and dispersion velocities of hypothetical volcanic density currents on Mars that were

TABLE II Flow parameters calculated for a range of possible explosive volcanic density currents on Mars*

FLOW DENSITY ρ_2 (g/cm^3)	SLOPE β (degrees)	HEIGHT h (m)	BOTTOM STRESS τ_0 ($dynes/cm^2$)	VELOCITY $\bar{u}$ (m/sec)
.2	10	10	1.3×10^4	25
		20	2.6×10^4	36
.6	5	5	9.7×10^3	9
		10	1.9×10^4	25

* All calculations assume a nominal suspended grain diameter D = .5cm, a drag coefficient c_f = .01, and a_0 = 83 . a_0 was determined empirically from the terrestrial data sets presented in this paper (Figure 5).

computed from equations (5), (7) and (12). The mean surface acceleration due to gravity on Mars is 371 cm/sec^2, 38% that of Earth's. The coefficient a_o was assumed to be equal to 83, the value determined empirically from our terrestrial models (Figure 5). Other variables being equal, a volcanic density flow on Mars should have a driving force about one third that of a terrestrial flow and travel at about three fifths the velocity. However, the minimum velocity necessary for a flow to suspend a bed of particles by either autosuspension or dispersive pressure is a function of settling velocity, and so also a function of gravitational acceleration. Pai, Hsieh and O'Keefe (1972) use an isothermal model to predict the fluidized behavior of lunar pyroclastic flows. Their analyses illustrate the effect of a lesser gravitational field on the pyroclastic flow process is to increase the average scale height of the flow. Any increase in height also increases the driving force and velocity terms (Equations 5, 7, 12) and may explain why channels on martian volcanoes that appear to have been eroded by explosive volcanic density currents are generally larger than similar terrestrial channels (Part II). Finally, the decrease in the terminal velocity of particles in a pyroclastic flow system which promotes grain support by autosuspension and dispersive pressure should cause the time during which a nuée ardente or base surge remains fluidized (and thus mobile) to be longer than that of a comparable terrestrial flow.

In summary, nuées ardentes and volcanic base surges should be possible on Mars provided a sufficient gas phase is generated by some process such as Vulcanian explosion of a separate gas phase or contribution of water vapor from an underground permafrost layer. The martian gravitational field would provide a smaller propelling force to such flows compared to Earth, but at the same time the average scale height of a martian flow would be larger than that of a terrestrial flow. Since these are opposing effects, the velocity and driving force terms for martian volcanic density currents should be comparable to terrestrial flows, and erosional and depositional processes on both planets should be closely analogous. Perhaps the only significant difference between martian and terrestrial volcanic density currents would be the distances traveled before a flow is completely dissipated. Terrestrial nuées ardentes and base surges typically travel a few to tens of kilometers, depending on their size and slopes, before loosing competence. Martian flows should travel and disperse debris over greater distances, however, because they have greater self-cohesion and remain fluidized longer. This observation may explain why martian composite volcanoes and tuff cones tend to have broader gentler slopes than similar constructs on Earth (Part II).

CONCLUSIONS

The calculations of specific nuée ardente flow parameters reported in this paper are intended to be interpreted as representative values and are not absolute. In a general way, however, they confirm the qualitative observations of Davies et al. (1978) and others about the nature of nuées ardentes.

(1) A nuée ardente is initially a low concentration, single layer, autosuspended, particle-gas dispersion with a high velocity that is principally a function of the downslope gravity force acting on the flow and the flow thickness. At this stage the nuée ardente has a large driving force and may erode channels on the steep upper slopes of its volcano.

(2) Once a nuée ardente moves onto gentler slopes, it can not remain autosuspended, but collapses into a high concentration modified grain flow in which the particle support mechanism is largely dispersive pressure generated by grain to grain interactions. Entrainment at the upper interface of the flow creates an overriding billowing cloud, and the nuée ardente becomes a two layer system.

(3) Deposition from the main underflow occurs by mass emplacement when the driving force of gravity becomes less than necessary to propel the flow. This "freezing" preserves the structure and texture of the flow prior to emplacement and thus explains the poor sorting and inverse grading found in the main flow unit of most ignimbrites. Deposition from the cloud is by slow grain by grain settling and produces a thin, blanketing, well-graded fall deposit.

(4) The particle flux model developed here for nuées ardentes may be applied to other types of sediment gravity flows, such as marine turbidity currents and mudflows. The model requires knowledge of the flow's path, changes in its velocity, and the rate that grains are

gained or lost with distance. From this information values for the flow densities and thicknesses can be estimated. One disadvantage of the present model is it does not allow for lateral spreading because the particle flux is on a unit width basis, but this can be accounted for in somewhat more elaborate models.

(5) An application of the model equations to hypothetical nuées ardentes or similar base surge flows in a martian environment indicates that the velocity and driving force terms for martian explosive volcanic density currents compare with values for terrestrial flows, but martian flows probably travel farther and disperse debris over greater distances.

REFERENCES

Anderson, T. and J.S. Flett, Report on the eruptions of the Soufrière, in St. Vincent, 1902, and on a visit to Montagne Pelée, in Martinique. Phil. Trans. R. Soc. Lond., A 200, 253-553, 1903.

Bagnold, R.A., Experiments on a gravity-free dispersion of large solid spheres in a Newtonian fluid under shear. Proc. R. Soc. Lond., A 225, 49-63, 1954.

Bagnold, R.A., The flow of cohesionless grains in fluids. Phil. Trans. R. Soc. Lond., A 249, 235-297, 1956.

Bagnold, R.A., Auto-suspension of transported sediment; turbidity currents. Proc. R. Soc. Lond., A 265, 315-319, 1962.

Bagnold, R.A., The nature of saltation and of "bed load" transport in water. Proc. R. Soc. Lond., A, 332, 473-504, 1973.

Benjamin, T.A., Gravity currents and related phenomena. J. Fluid Mech., 31, 209-248, 1968.

Davies, D.K., M.W. Quearry, and S.B. Bonis, Glowing avalanches from the 1974 eruption of the volcano Fuego, Guatemala. Bull. Geol. Soc. Am., 89, 369-384, 1978.

Fisher, R.V., Mechanism of deposition from pyroclastic flows. Am. J. Sci., 264, 350-363, 1966.

Fisher, R.V., Features of coarse-grained, high-concentration fluids and their deposits. J. Sedim. Petrol., 41, 916-927, 1971.

Fisher, R.V., and J.M. Mattinson, Wheeler Gorge Turbidite-conglomerate series, California; inverse grading. J. Sedim. Petrol., 38, 1013-1023, 1968.

Hampton, M.A., Competence of fine-grained debris flows. J. Sedim. Petrol., 45, 834-844, 1975.

Henderson, F.M., Open Channel Flow. Macmillan Co., New York, 522 pp., 1966.

Johnson, M.A., Turbidity currents. Oceanogr. Mar. Biol. Ann. Rev., 2, 31-43, 1964.

Kersey, D.G. and K.J. Hsu, Energy relationships of density-current flows: an experimental investigation. Sedimentology, 23, 761-789, 1976.

Keulegan, G.H., Thirteenth progress report on model laws for density currents. ;An experimen-al study of the motion of saline water from locks into fresh water channels. U.S. Natl. Bur. Stand. Rept. 5168, 1957.

Keulegan, G.H., Twelfth progress report on model laws for density currents. The motion of saline fronts in still water. U.S. Natl. Bur. Stand. Rept. 5831, 1958.

Komar, P.D., The channelized flow of turbidity currents with application to Monterey Deep-Sea Fan Channel. J. Geophys. Res., 74, 4544-4556, 1969.

Komar, P.D., Hydraulic jumps in turbidity currents. Bull. Geol. Soc. Am., 82, 1477-1488, 1971.

Komar, P.D., Relative significance of head and body spill from a channelized turbidity current. Bull. Geol. Soc. Am., 83, 1151-1156.

Komar, P.D., Computer simulation of turbidity current flow and study of deep-sea channels and fan sedimentation. In: The Sea: Ideas and Observations on Progress in the Study of the Seas, 6. (Ed. by E.D. Goldberg) Wiley & Sons, 603-621, 1977.

Komar, P.D., Comparisons of the hydraulics of water flows in martian outflow channels with flows of similar scale on Earth. In Press. 1978.

Kuenen, Ph.H., Turbidity currents of high density. Int. Geol. Congr. Rept. 18th Sess., Great Britain, pt 8, 44-52, 1950.

Kuenen, Ph.H., Estimated size of the Grand Banks turbidity current. Am. J. Sci., 250,874, 1952.

Lacroix, A., L'eruption de la montagne Pelée en janier 1903. Acad. Sci. (Paris) Comptes rendus, 136, 442-445, 1903.

Lowe, D.R., Grain flow and grain flow deposits. Jour. Sed. Pet., 46, 188-199, 1976.

Macdonald, G.A. and A. Alcaraz, Nuées ardentes of the 1948-1953 eruption of Hibok-Hibok. Bull. Volcanol. Ser. 2, 18, 169-178.

McTaggart, K.C., The mobility of nuees ardentes. Am. J. Sci., 258, 369-382, 1960.

Middleton, G.V., Experiments on density and turbidity currents. Parts I-III. Can. J. Earth Sci. 3, 523-546, 627-637, and 4, 475-505, 1966-1967.

Middleton, G.V., Experimental studies related to the problems of flysch sedimentation. Geol. Assoc. Canada Spec. Paper 7, 253-272, 1970.

Middleton, G.V. and M.A. Hampton, Subaqueous sediment transport and deposition by sediment gravity flows. In: Marine Sediment Transport and Environmental Management. (Ed. by Stanley and Swift) Wiley & Sons, New York, 197-218, 1976.

Middleton, G.V. and J.B. Southard, Sediment gravity flows. Chapter 8 in: Mechanics of Sediment Movement. SEPM Short Course, No. 3, Binghamton, 1977.

Moore, J.G. and W.G. Melson, Nuées ardentes of the 1968 eruption of Mayon Volcano, Philippines. Bull. Volcanol., 33, 600-620.

Pai, S.I., T. Hsieh, and J.A. O'Keefe, Lunar ash flows: isothermal approximation. J. Geophys. Res., 77, 3631-3649, 1972.

Schlichting, H., Boundary Layer Theory, McGraw-Hill, New York, 534-565, 1960.

Seiff, A. and D.B. Kirk, Structure of Mars' atmosphere up to 100 kilometers from the entry measurements of Viking 2. Science, 194, 1300-1302, 1976.

Sparks, R.S.J., Grain size variations in ignimbrites and implications for the transport of pyroclastic flows. Sedimentology, 23, 147-188, 1976.

Sparks, R.S.J., S. Self, and G.P.L. Walker, Products of ignimbrite eruptions. Geology, 1, 115-118, 1973.

Sparks, R.S.J. and G.P.L. Walker, The ground surge deposit: a third type of pyroclastic rock. Nature Phy. Sci., 241, 62-64.

Sparks, R.S.J., L. Wilson, and . Hulme, Theoretical modeling of the generation, movement, and emplacement of pyroclastic flows by column collapse. J. Geophys. Res., 83, 1727-1739, 1978.

Stith, J.L., P.V. Hobbs, and L.F. Radke, Observations of a nuée ardente from St. Augustine Volcano. Unpublished Paper. 1977.

Tazieff, H., New investigations on eruptive gases. Bull. Volcanol., 34, 421-438, 1970.

Walker, G.P.L., Grain-size characteristics of pyroclastic deposits. Jour. Geology, 79, 696-714, 1971.

Wilson, L., Explosive volcanic eruptions-III. Plinian eruption columns. Geophys. J. Roy. Astron. Soc., 45, 543-556, 1976.